CONTRACTOR REPORT

SAND82-7102
Unlimited Release
UC-63c

Photovoltaic Concentrator With Plastic Film Reflector

Final Report

Boeing Engineering and Construction Company
A Division of The Boeing Company
Seattle, Washington 98124

Prepared by Sandia National Laboratories Albuquerque, New Mexico 87185
and Livermore, California 94550 for the United States Department of Energy
under Contract DE-AC04-76DP00789

Printed June 1982

When printing a copy of any digitized SAND Report, you are required to update the markings to current standards.

Issued by Sandia National Laboratories, operated for the United States Department of Energy by Sandia Corporation.

NOTICE: This report was prepared as an account of work sponsored by an agency of the United States Government. Neither the United States Government nor any agency thereof, nor any of their employees, nor any of their contractors, subcontractors, or their employees, makes any warranty, express or implied, or assumes any legal liability or responsibility for the accuracy, completeness, or usefulness of any information, apparatus, product, or process disclosed, or represents that its use would not infringe privately owned rights. Reference herein to any specific commercial product, process, or service by trade name, trademark, manufacturer, or otherwise, does not necessarily constitute or imply its endorsement, recommendation, or favoring by the United States Government, any agency thereof or any of their contractors or subcontractors. The views and opinions expressed herein do not necessarily state or reflect those of the United States Government, any agency thereof or any of their contractors or subcontractors.

Printed in the United States of America
Available from
National Technical Information Service
U.S. Department of Commerce
5285 Port Royal Road
Springfield, VA 22161

NTIS price codes
Printed copy: A05
Microfiche copy: A01

SAND82-7102
Unlimited Release
Printed August

Distribution
Category UC-63c

Photovoltaic Concentrator With Plastic Film Reflector

Prepared for
Sandia National Laboratories
Albuquerque, NM

by

Boeing Engineering and Construction Company
A Division of the Boeing Company
Seattle, Washington 98124

Under Contract No. 13-5060

Abstract

Boeing Engineering has designed, fabricated, and tested a 4m diameter reflective film, parabolic dish concentrator proposed for use with a photovoltaic array. The concentrator is made from aluminized film gores (wedge shaped pieces) that are taped together along their edges to form a dish. The shape of the dish is maintained by a pressure difference between the front and back. The deep dish was designed to illuminate a cylindrical receiver populated by solar cells with a geometric concentration ratio of 145. Three full scale dishes were made in sequence, each using improvements suggested by the previous design. They were tested with a laser to determine surface errors and flux uniformity on the target. Boeing was unable to achieve a flux uniformity good enough for a photovoltaic application and the project was ended.

FOREWORD

This document is the final report issued under Sandia Laboratories Contract 13-5060. The objective of this contract was to design, fabricate and evaluate a photovoltaic concentrator utilizing a plastic film reflector. Task I, II, III, and IV, as designated in the statement of work, were initiated on May 1, 1979, and completed on December 31, 1979. Tasks V, VI, and VII were initiated on May 1, 1980, and were completed on November 1, 1980. Technical management at Sandia was performed by Mr. Michael Edenburn. Program management at Boeing Engineering and Construction (BEC) was performed by Mr. Donald K. Zimmerman. Mr. John Laakso was engineering manager. BEC engineering personnel contributing to the project were Mr. Harry Dursch, Mr. David Kirkbride, Mr. Henry Mayorga, and Ms. Cheryl Warner.

TABLE OF CONTENTS

		PAGE
NOTICE		i
FOREWORD		ii
1.0	EXECUTIVE SUMMARY	1
2.0	INTRODUCTION	10
3.0	CONCENTRATOR DESIGN	11
3.1	System Description	11
3.2	Concentrator Design Features	14
3.2.1	Enclosure	14
3.2.2	Photovoltaic Cell Receiver	18
3.2.3	Reflector Support Shell	24
3.2.4	Yoke, Drive and Control System	24
3.3	Concentrator Prototype Design Features	26
3.3.1	Prototype Reflector Support Shell	26
3.3.2	Prototype Photovoltaic Module Target	28
4.0	REFLECTOR DESIGN	29
4.1	Reflector Design Features	29
4.2	Reflector Contour Analysis	31
5.0	PROTOTYPE CONCENTRATOR FABRICATION	36
5.1	Reflector Fabrication Techniques	36
5.2	Reflector Fabrication Results	44
5.3	Concentrator Assembly and Alignment	54

6.0 PROTOTYPE CONCENTRATOR TESTING 61
6.1 Outdoor Testing Plan 61
6.2 Indoor Testing 61
6.2.1 Test Procedure 61
6.2.2 Test Data Analysis 63
6.2.3 Test Results 65

7.0 CONCLUSIONS 74

8.0 REFERENCES 76

1.0 EXECUTIVE SUMMARY

The program described in this report investigated the feasibility of using a pressure-stabilized plastic film with a reflective coating as a low cost, high efficiency concentrator for a photovoltaic array. One approach to achieving cost reductions in photovoltaic systems is to concentrate the incident sunlight onto the receiver, increasing its power output and reducing the area requirements and cost of the photovoltaic cells. High cost of the solar cells comprising a photovoltaic module has been the major obstacle to practical use of photovoltaics for terrestial applications. A concentrating photovoltaic array can be effective if the cost of the concentrator is below the cost of the solar cells replaced. The use of plastic films helps attain this goal by making possible cost reductions in the reflector, supporting framework and drive systems.

Previous work the Boeing Engineering and Construction Company (BEC) performed in designing, fabricating, and evaluating plastic film concentrators provided the basis for this program. Figure 1-1 is a 2 m diameter parabolic reflector fabricated under a previous contract with Sandia National Laboratories, undergoing a solar simulation test [1], [2] . This early work established that 18 tapered triangular forms called gores joined together at the edges, could be used to achieve a high efficiency, high concentration ratio parabolic plastic film reflector. The reflector was fabricated from aluminized polyester gores and stabilized to its parabolic shape with a small differential pressure between the front and back of the film. Under the same contract, a conceptual photovoltaic concentrator design was developed, shown in Figure 1-2. This design provided the basis from which the current design evolved. The photovoltaic receiver was supported by a cantilever structure, which eliminates shadowing of the reflector from support struts, and a pedestal support. A modified parabolic plastic film reflector provided the illumination on the receiver. The reflector film was supported by a lightweight fiberglass shell and stabilized by slightly reducing the air pressure between the reflector film and its support shell. Concentrating photovoltaic cells spanned the full width of the receiver surface. A 5.2 m diameter, transparent, spherical, air supported plastic film enclosure protected the array from the environment (wind loads, precipitation,

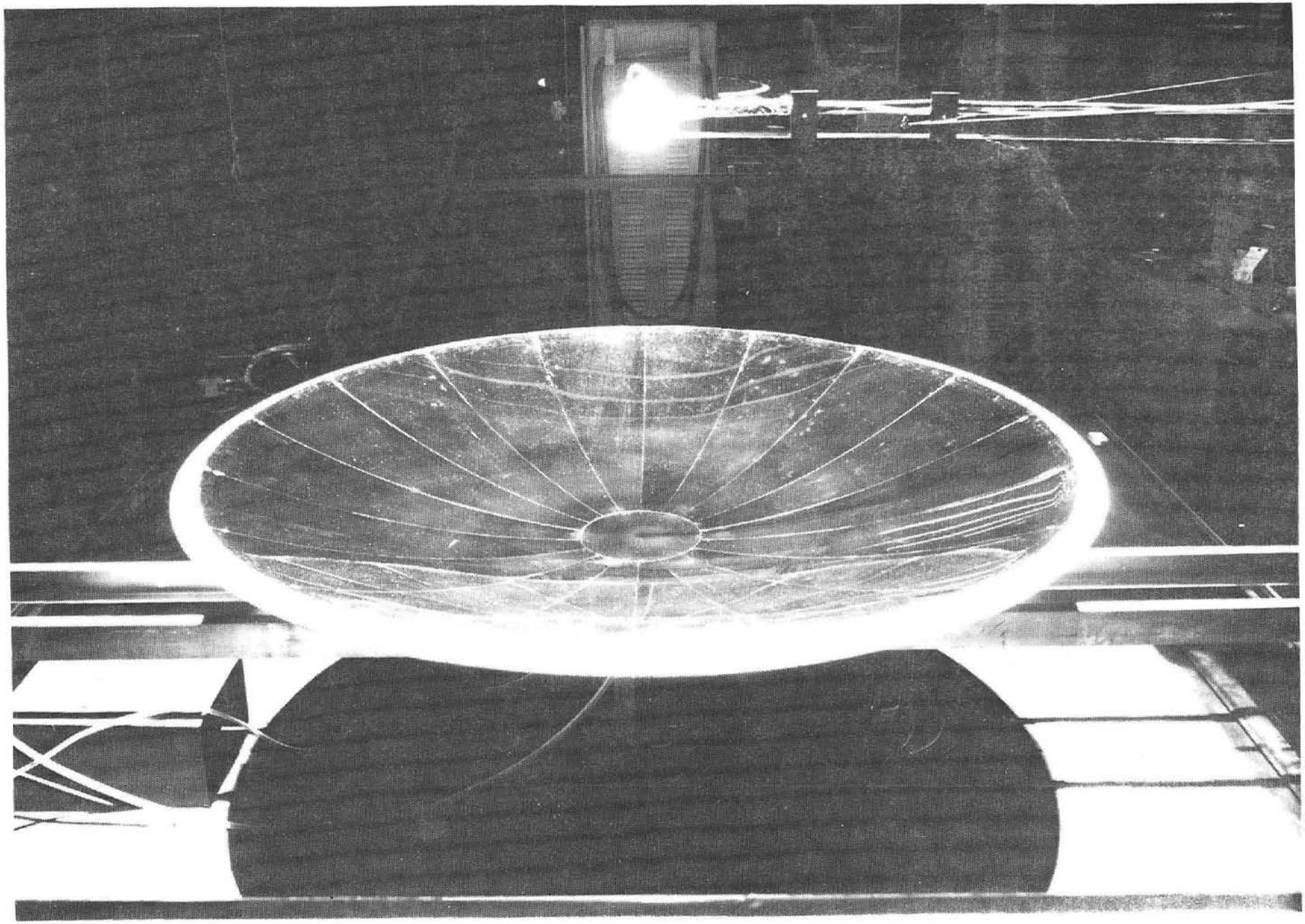

Figure 1-1: Two Meter Diameter Plastic Film Parabolic Concentrator

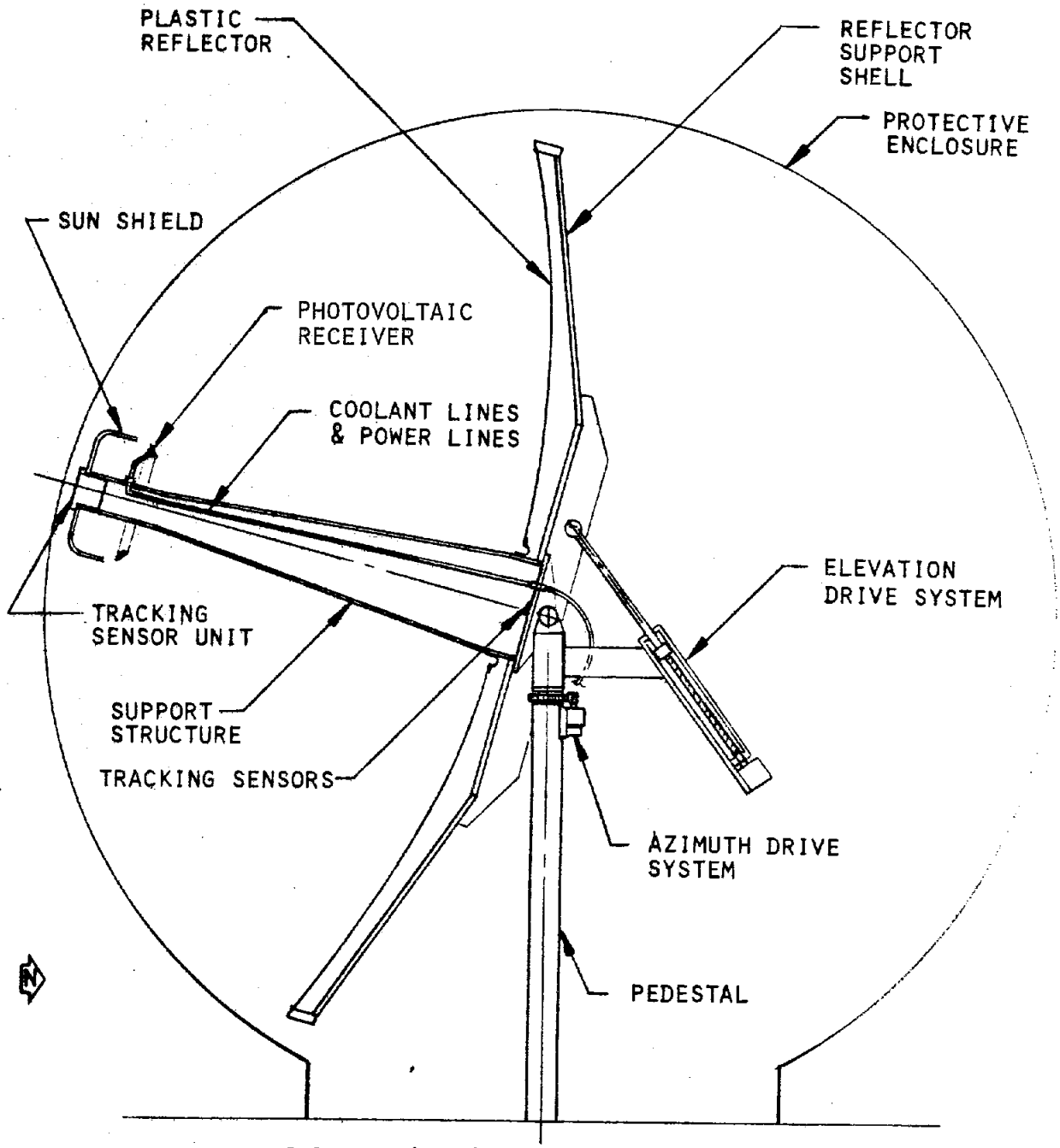

Figure 1-2: Previous Concentrator Design

particulate accumulation). This allowed the supporting structure to be lightweight and inexpensive. The plastic film enclosure concept was adapted from BEC's plastic film heliostat program [3]. The size selected was based on the 5.2 m diameter enclosures BEC used for subscale heliostat experiments. Figure 3-4 shows two of these enclosures undergoing outdoor exposure testing in northeast Oregon.

Figure 1-3 shows a 5.2 m diameter parabolic point focus solar reflector undergoing a laser ray trace to characterize its surface errors [4] . The reflector was fabricated using eighteen gore segments of aluminized polyester, which was essentially a scale-up of the 2m reflector shown in Figure 1-1 . The reflector was supported by a wood box-section ring with a front surface of clear polyester which enabled the reflector to be pressurized. 1728 data points were taken using a laser ray trace optical test. The reflector had an overall RMS surface error of 7.57 milliradians (mrad) with a random RMS surface error (radial systematic errors removed) of 5.52 mrad. This reflector again verified the use of large gore angles and provided the initial reflector fabrication techniques that were used during this program.

The main objective of the Photovoltaic Concentrator with Plastic Film Reflector program reported herein was to determine the most practical configuration for a photovoltaic receiver and optimize the reflector shape to produce uniform illumination of the receiver. Several reflectors were built to experimentally determine the flux on the receiver using the laser ray trace test technique. Also a conceptual design of a photovoltaic concentrator was developed using the selected reflector configuration.

Various combinations of reflector shapes and photovoltaic module geometries were analyzed using a ray trace optical computer model. The best configuration was found to have a cylindrical receiver and a deep dish reflector capable of providing uniform flux on the cylindrical receiver surface. This configuration provided a good compromise between energy capture, depth of reflector, solar cell layout on the receiver, energy incidence angle on the cells, and active reflector area. The reflector had a geometric concentration ratio of 145, selected to achieve 100 suns on the receiver. The photovoltaic receiver was covered by solar cells (each measuring 104 5.33 cm x 1.8 cm) providing an expected output of 1 kW at 100 suns.

Figure 1-3: Previous Parabolic Reflector Optical Test

A steel tube yoke provided the gimbaling required for the azimuth-elevation sun tracking capabilities. The 5.2 m diameter enclosure limited the diameter of the reflector to 4 m. Figure 1-4 is a drawing of the final configuration.

A prototype concentrator was fabricated to demonstrate and evaluate the conceptual design. The prototype reflectors were fabricated with gore-shaped segments of .05 mm (.002 inch) thick aluminized polyester film, which had a specular reflectance of 86% at a cone angle of .14° (2.5 mr). The reflector surface shape is established by the gore shape, cut with the aid of an accurately fabricated gore template, and careful aligning of the gores before taping the seams. This eliminates the need for a highly accurate lay-up tool. The reflector was supported by a lightweight fiberglass shell and stabilized with a slight negative pressure. Figure 1-5 shows the concentrator pressurized to its operating pressure and undergoing a laser ray trace test. Three 4 m diameter and two 2 m diameter reflectors were fabricated and installed on their respective support shells. Each reflector was evaluated, and changes were incorporated into the subsequent reflector to improve performance. Optical evaluations of the reflectors were performed using a laser ray trace technique in order to determine local variations in surface error and to relate observed errors with physical features on the reflector. The laser ray was reflected from the reflector surface onto a simulated receiver. The observed laser image on the module was then compared to the design intercept point to determine the local surface error, and the density of the images on the module provided a map of the expected solar intensity on the solar cells.

Results of the fabrication and testing showed that the deep-dish concentrator configuration was considerably more difficult to implement than the previously evaluated shallow paraboloids. An initial attempt using 20° gore angles showed substantial surface errors caused by wrinkling, especially along the gore seams. In an effort to determine the cause of these wrinkles, a NASTRAN computer model of the reflector was developed. The analysis indicated that the wrinkling would become acceptably small by changing to a 15° gore angle and by switching to a pressurized mounting technique when installing the reflector to the reflector support shell. A second full scale reflector was built using these improvements, but again with disappointing results. An extensive review led to a change in fabrication techniques.

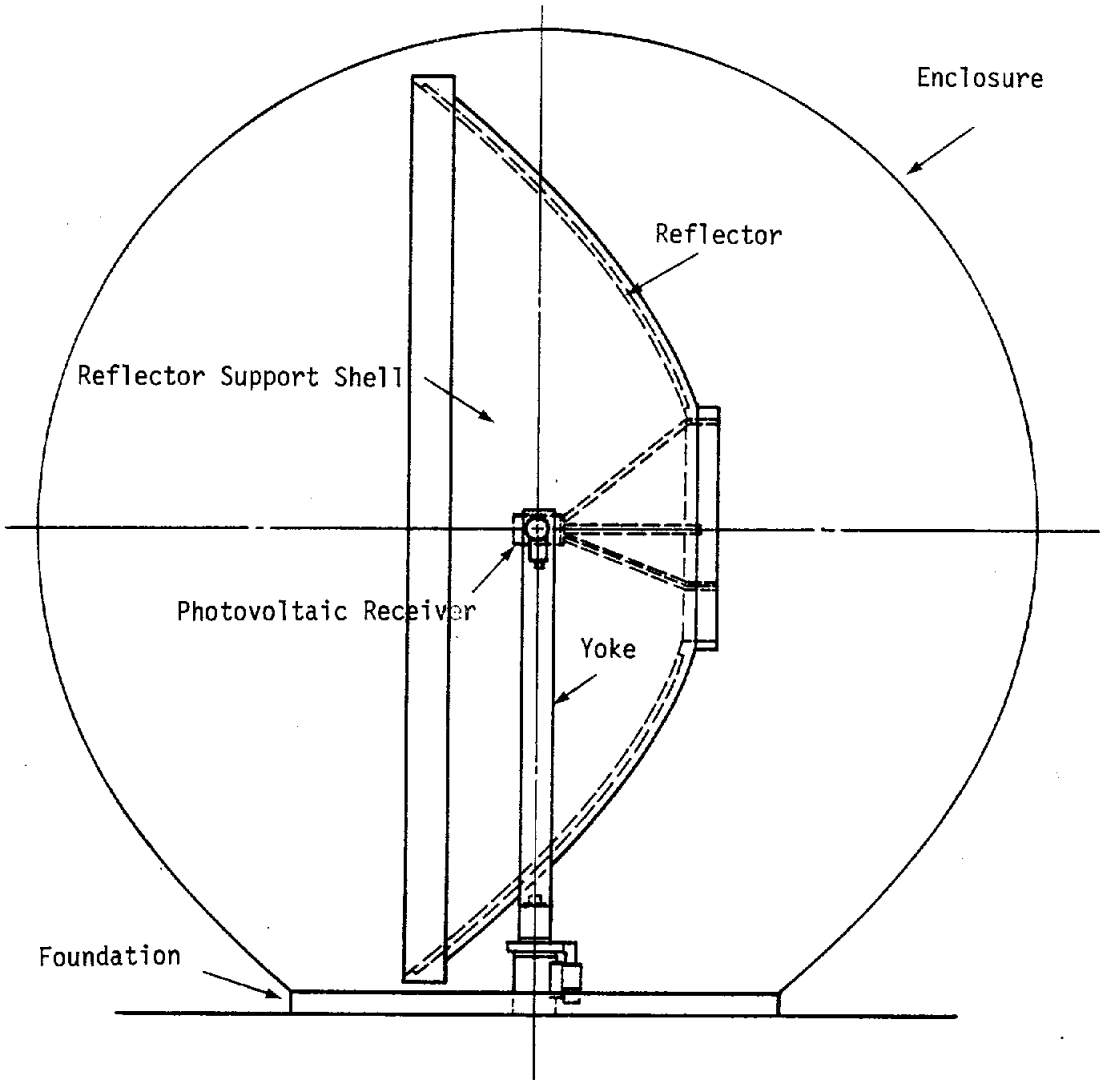

Figure 1-4: Photovoltaic Concentrator Final Configuration

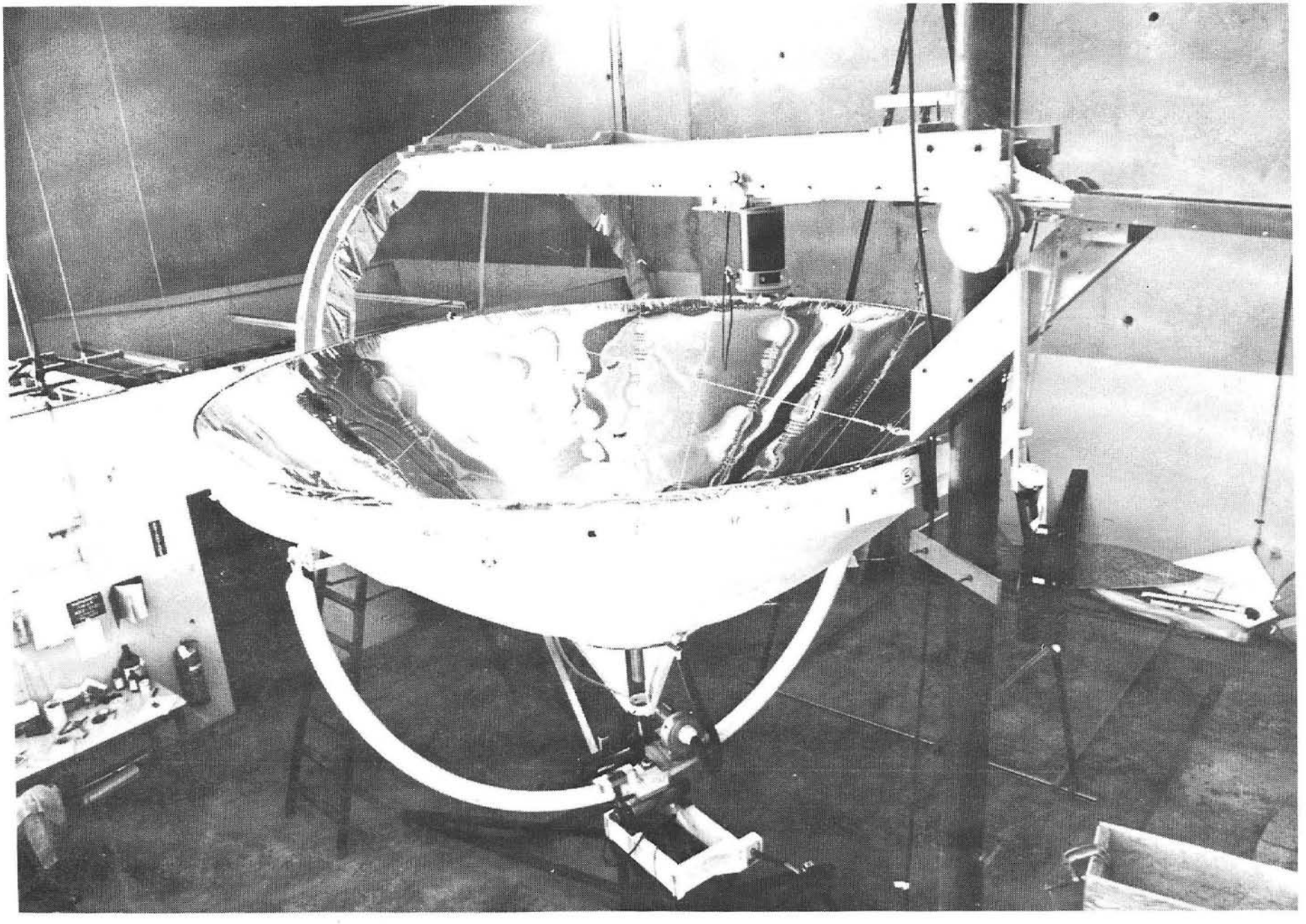

Figure 1-5: Prototype Concentrator in Laser Ray Trace Test

The third full-scale reflector was built at a sail loft by personnel experienced in joining panels with similar radii of curvatures. Panels were joined on a flat surface which permitted close observation and, therefore, increased gore joining precision. This reflector was built as accurately as possible without the use of expensive, high accuracy lay-up tooling. The results improved but the reflector still provided a nonuniform flux distribution on the receiver. The gore centerlines of the reflector had an overall RMS surface error of 12.95 mrad and a random RMS surface error of 7.89 mrad. It was judged that the nonuniform flux profile was unacceptable for a photovoltaic application and the project was ended.

2.0 INTRODUCTION

An investigation into the use of plastic film for a photovoltaic concentrator is described. This program draws on much of the design studies, materials evaluation and fabrication experience gained in BEC's previous work on ERDA/DOE solar development programs [1,2,3,4].

The BEC concentrator design concept is based on a reflector fabricated from gore shaped segments of metallized plastic film. The reflector is supported by a conical shaped shell and stabilized with a small reduction in pressure between the shell and reflector. The reflector and reflector support shell are supported by a steel tube yoke which provides the necessary gimbaling required for azimuth-elevation sun tracking. The concentrator is protected from the environment by a transparent plastic film enclosure, adopted from a BEC heliostat program [3].

The Photovoltaic Concentrator with Plastic Film Reflector program was composed of 4 main tasks:

1) Determine the most practical configuration for a dish concentrator and photovoltaic receiver with a concentration ratio between 70 and 200 and optimize the reflector shape to produce uniform illumination on the receiver.
2) Prepare a detailed design of the concentrator which has all the necessary mounting interfaces to be used in a complete, tracking, enclosed array. Design the other components in the system (enclosure, structure, tracking, receiver) to the extent necessary to prepare the detailed concentrator design.
3) Fabricate the concentrator according to the specifications arrived at in task 2.
4) Experimentally determine the illumination flux on the concentrator's receiver using a laser ray trace and a real sun test.

3.0 CONCENTRATOR DESIGN

3.1 System Description

The concentrator system conceptual design consists of the following components which are illustrated in Figures 3-1 and 3-2.

- Plastic film enclosure dome
- Plastic film reflector
- Reflector support shell (fiberglass sandwich construction)
- Photovoltaic cell receiver (at cylindrical focal plane)
- Receiver support tripod
- Reflector support yoke (steel tube)
- Receiver cooling lines
- Enclosure foundation
- Output power bus
- Enclosure/reflector pressurization and filtration unit
- Azimuth and elevation tracking drives
- Tracking and pressure control unit (microprocessor based)

Key design considerations are:

1) The enclosure isolates the concentrator components from wind loading and the environment which results in low overall concentrator weight and eliminates cleaning of the reflector surface.
2) The yoke bearings are located at the reflector center of gravity axis for low drive power requirements.
3) The reflector support shell has high structural rigidity because of the high shell curvature and is constructed from lightweight fiberglass sandwich construction.

The photovoltaic cell receiver consists of a fluid-cooled metallic cylinder on which rectangular cells are mounted. Cell interconnections would be arranged to minimize performance loss due to flux fall off at the receiver's ends and due to cell malfunction. The receiver and reflector are sized to produce a nominal 100 sun concentration.

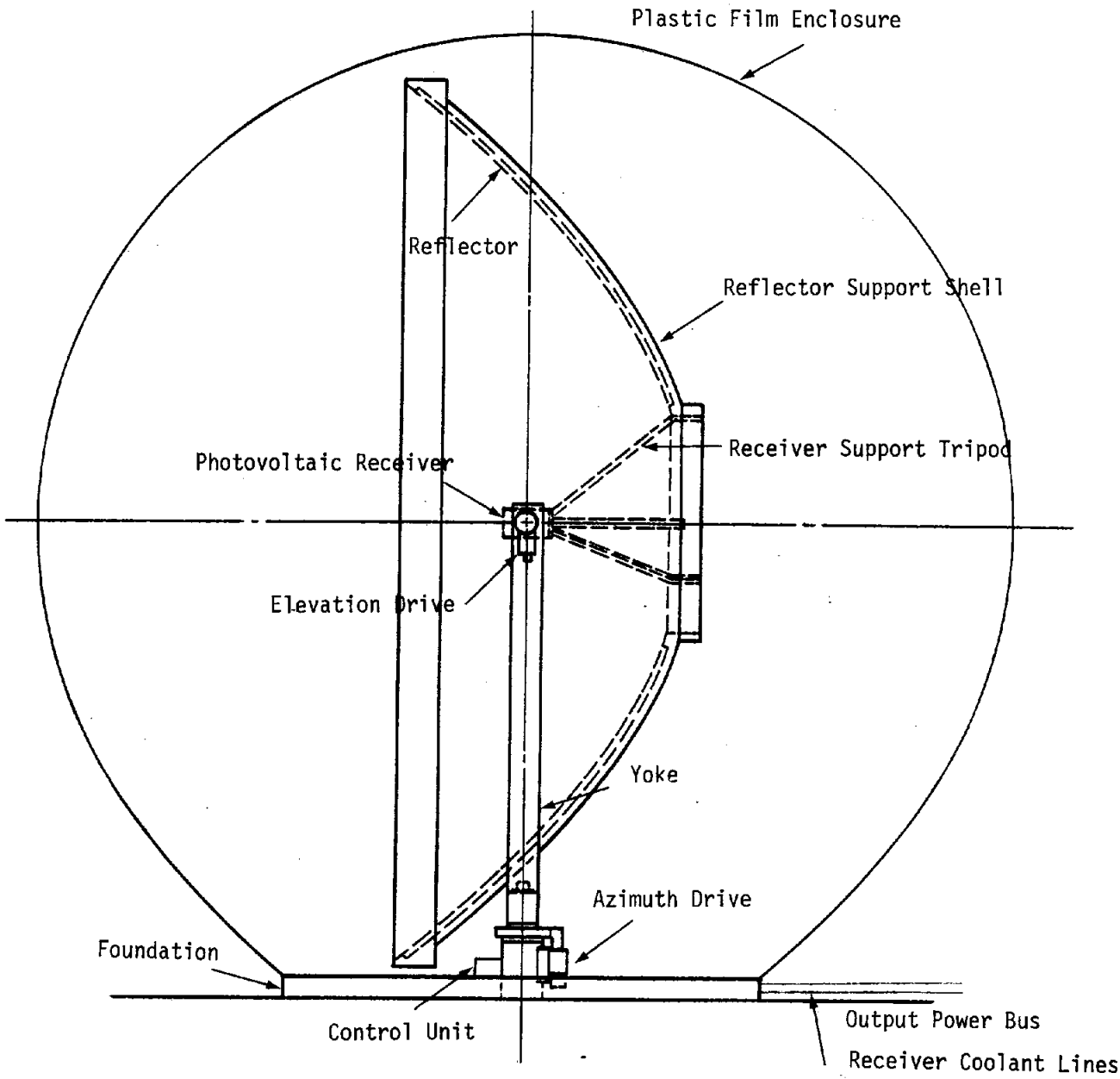

Figure 3-1: Photovoltaic Concentrator Side View

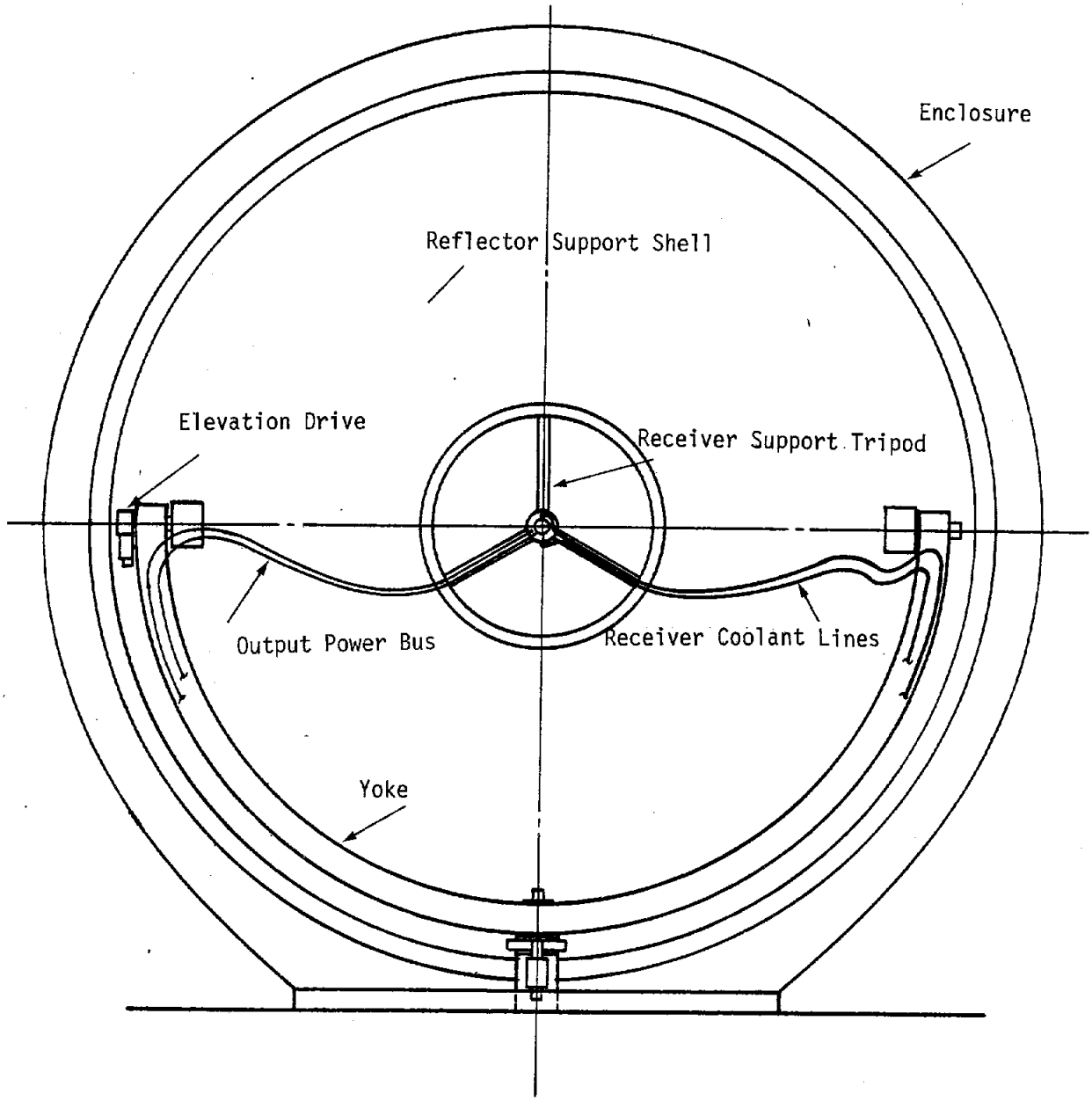

Figure 3-2: Photovoltaic Concentrator Back View

The major components of the concentrator are described in greater detail in the following sections.

3.2 Concentrator Design Features

3.2.1 Enclosure

The enclosure is a spherical, transparent, air supported plastic film structure. The enclosure protects the concentrator from the environment (wind loads, precipitation, etc.) and, with a filtration system, eliminates the need for cleaning the reflector surface. Figure 3-3 shows the enclosure configuration. A seam on the north side of the enclosure allows installation in the field over a completed concentrator. An access door would be installed to permit subsequent maintenance using an air lock. A rope bead at the enclosure's edge is fastened to the foundation by means of a continous clamp.

Shown in Figure 3-4 are two 5.2 m (17 ft) diameter gore formed domes fabricated by Sheldahl under contract with BEC and installed in Boardman, Oregon. The dome on the right is fabricated from ICI internally UV stabilized polyester. It failed during a 22 m/s (50 mph) wind storm after 23 months exposure. During this time it had survived severe snow loading, 31 m/s (70 mph) wind storms and volcanic ash. The dome on the left was fabricated from Celanese UV stabilized polyester and failed after 13 months exposure due to unknown causes. The domes are pressurized to 379 Pa (.055 psi) which enables the dome to survive a 40 m/s (90 mph) wind. The 5.2 m diameter enclosure was selected for the concentrator prototype design because of the experience and success in fabrication and installation of this size. The enclosure limits the maximum reflector diameter of the selected configuration to 4 m.

The current baseline material for the enclosure is a Pennwalt fluorocarbon called Kynar®. After an equivalent of over 15 years solar exposure (accelerated testing), and 2 years of real time desert exposure, Kynar has exhibited little or no mechanical or optical degradation as shown in Figure 3-5 [5].

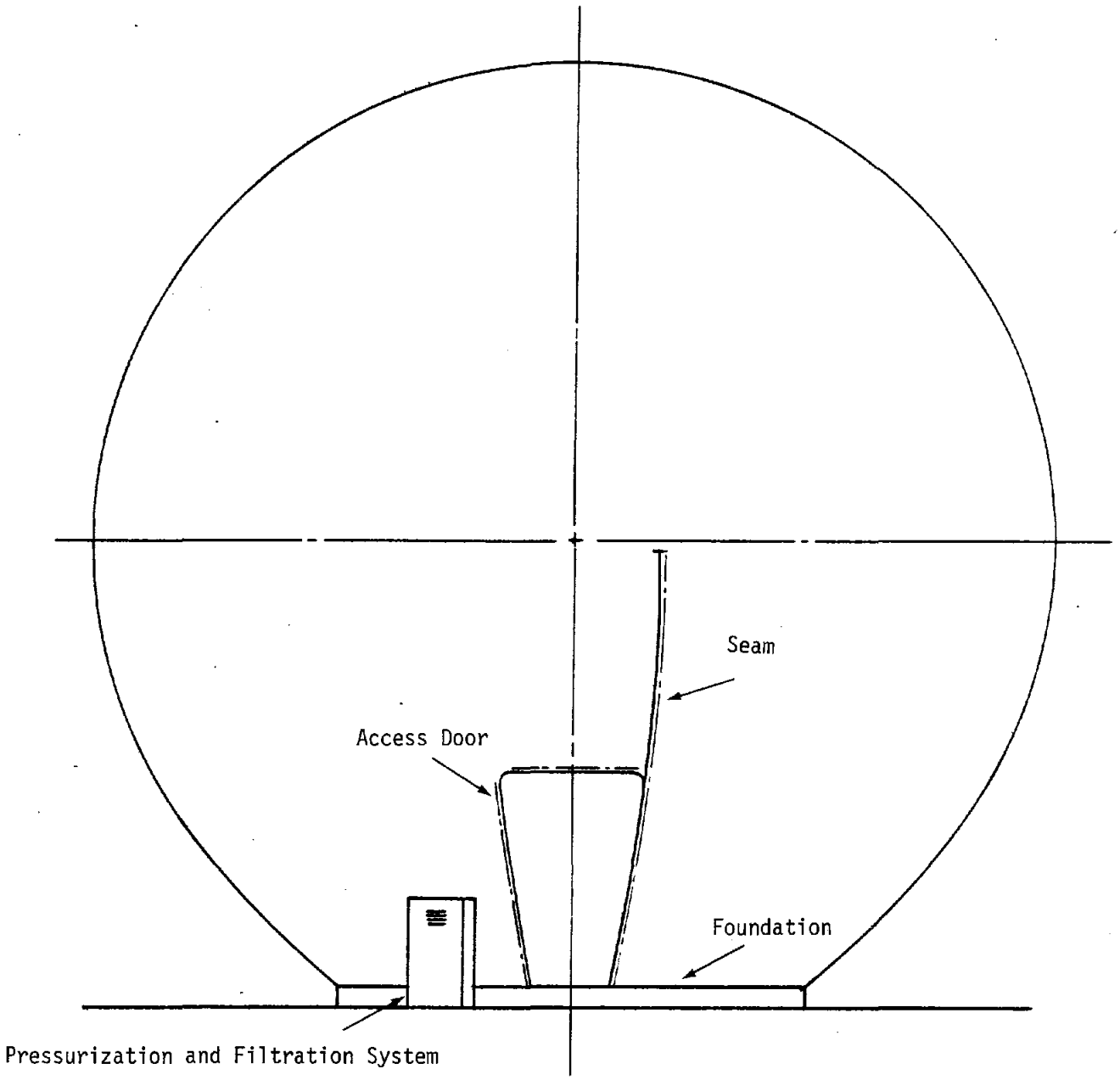

Figure 3-3: Photovoltaic Concentrator Enclosure

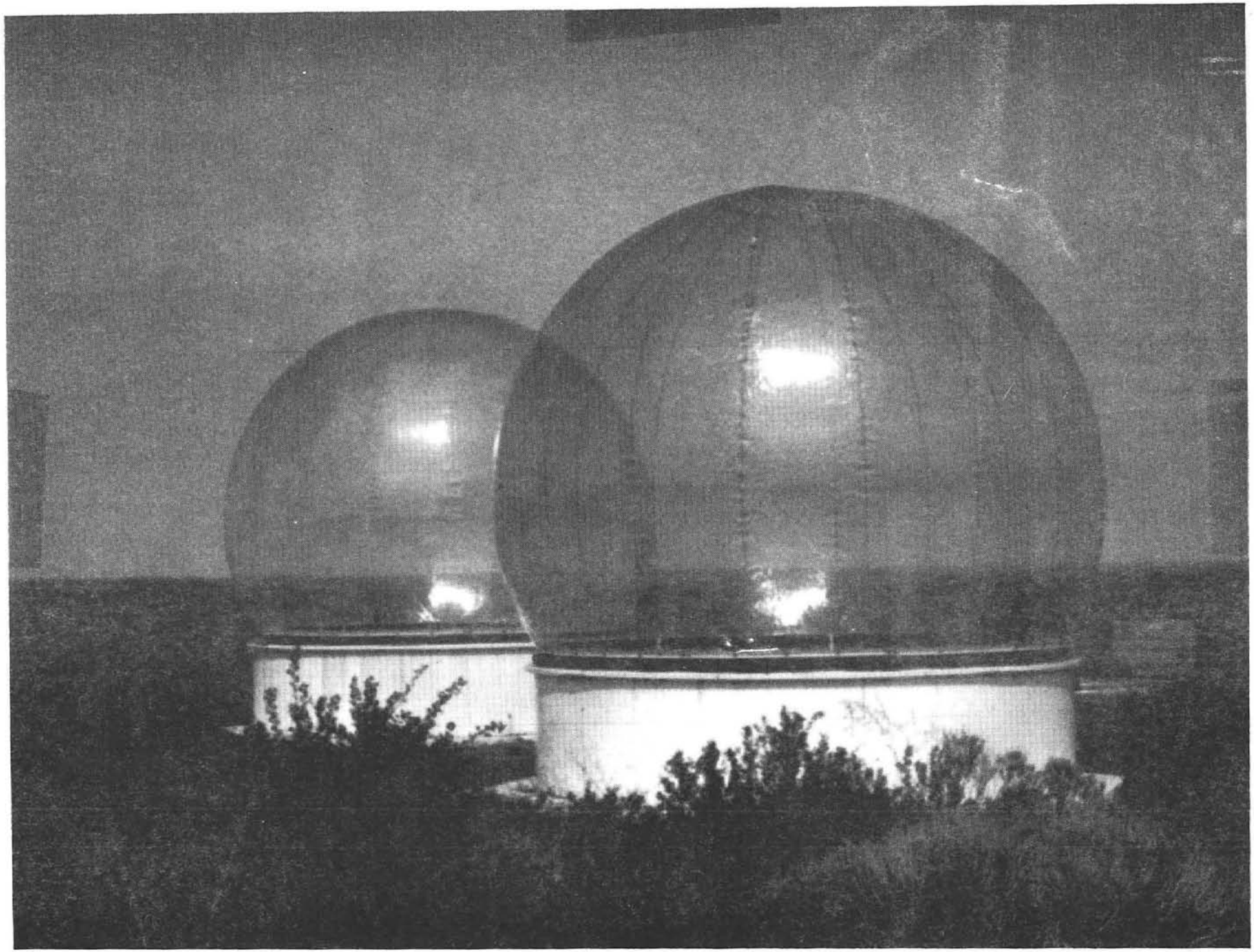

Figure 3-4: Polyester Enclosures Installed at Boardman, Oregon

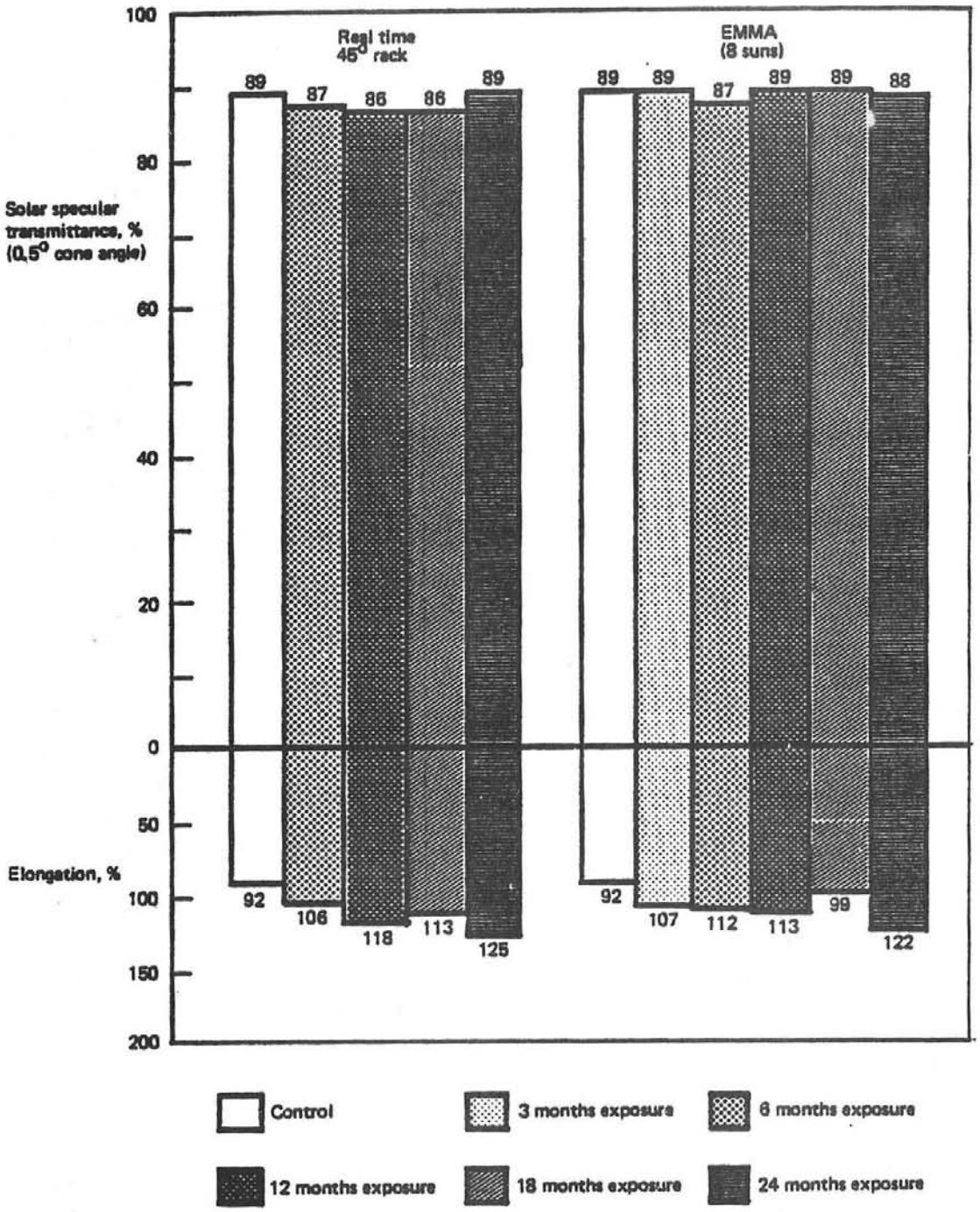

Figure 3-5: Kynar Exposure Testing Results

3.2.2 Photovoltaic Cell Receiver

The photovoltaic receiver geometry was defined by an interactive computer-aided design procedure that computed concentrator geometry for various receiver shape, size and location options. A geometric concentration ratio of 150 was initially selected for receiver sizing in configuration trade studies. This value will be reduced to about 100 due to transmittance and reflectance losses.

Several conceptual receiver configurations were evaluated in terms of practical cell geometry, interconnections, cooling, required concentrator accuracy, production method and ease of servicing. These receiver concepts basically are:

- cylindrical array with rectangular cells

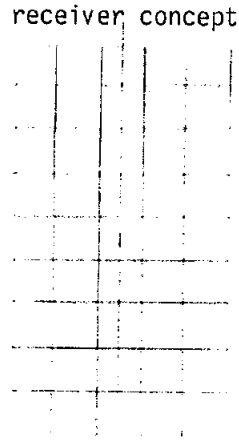

- conical array with trapezoidal cell

- flat circular array with trapezoidal cells

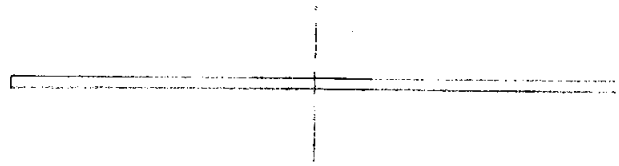

The flat circular receiver was eliminated as a contender because of non-uniform flux distribution and complicated cell lay-out and interconnections.

Concentrator geometries that result from the cylindrical and conical shapes are illustrated in Figure 3-6. Case 1, having a conical shaped receiver and trapezoidal cells, represents the maximum receiver elevation permitted by enclosure clearance. A conical receiver configuration is required to maintain acceptable incidence angles of the energy onto the cells. The remaining three cases, with shorter focal lengths, allow transition to cylindrical receivers.

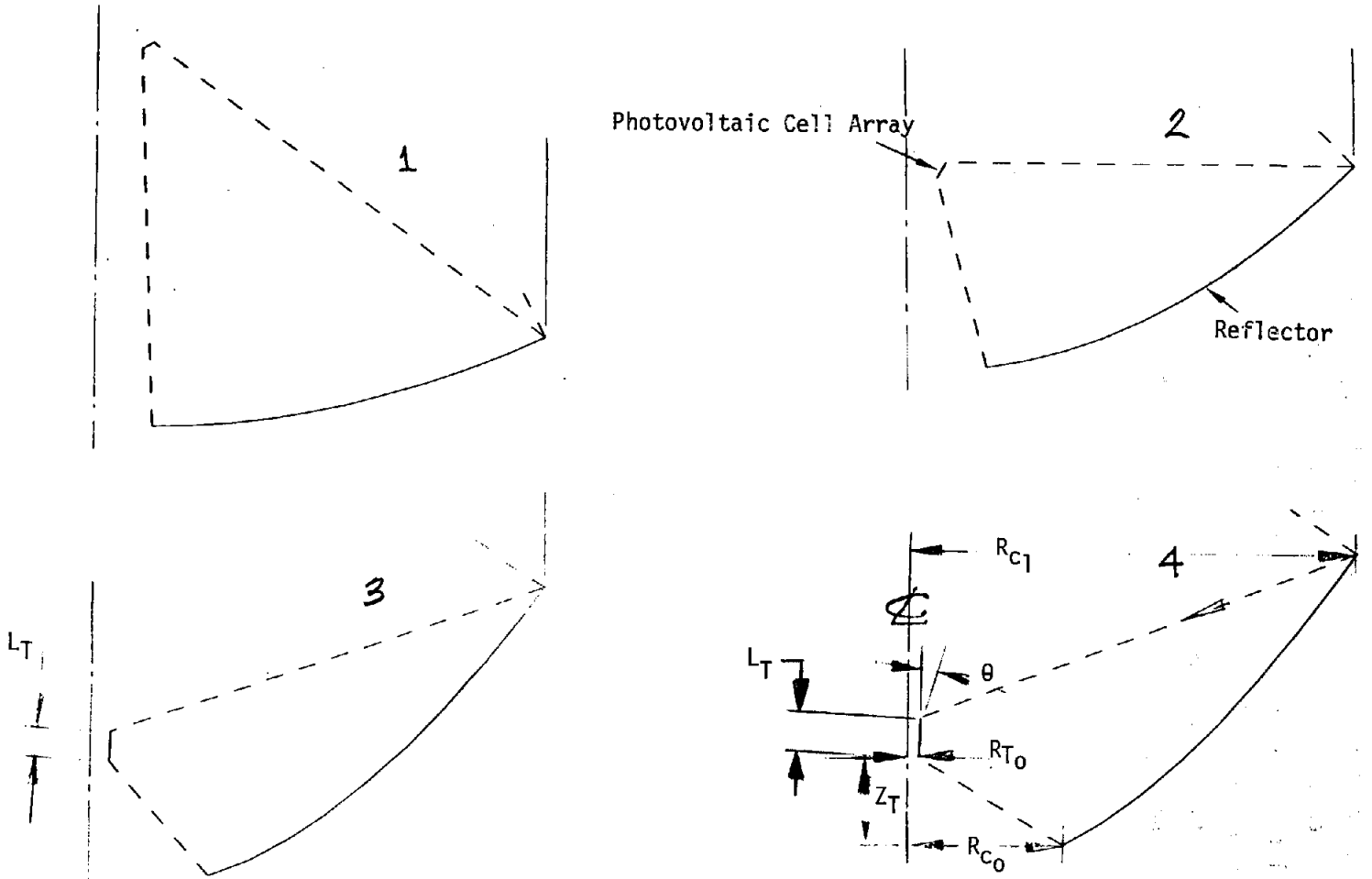

Figure 3-6: Reflector and Receiver Configuration Options

The reflector and receiver geometry will affect the concentrator efficiency because of the finite size of the sun's image on the cells and optical and tracking errors that may be present. An analysis of flux distribution was performed using a ray trace code adapted from previous work. Results of this analysis and the geometric parameters used are shown in Figure 3-7. Case 3 was selected for development based on these results along with the following considerations:

- The cells are all alike and have a rectangular configuration which offers high wafer yield.

- Each ring of cells can be connected in series and the rings can be connected in parallel. This minimizes current drop due to possible flux intensity variations along the cylindrical receiver.

- The cylindrical shape has a long vertical aspect ratio which results in reduced flux spillage.

- The cylindrical shape requires a deep concentrator dish configuration which is compatible with the spherical enclosure envelope.

- A cylindrical receiver structure can be easily fabricated from a copper extrusion with flat facets (for mounting cells) and integral coolant passages. The receiver mounting facets (1) allow access to cell interconnections for installation and repair and (2) permit use of interconnection details that have compliance for thermal expansion, (3) have good cooling of interconnects that are not directly illuminated, and (4) offer broad cell mounting area for good cell cooling.

Figure 3-8 is the selected concentrator configuration. It differs slightly from Case 3 because the final geometric concentration ratio was changed from 150 to 144.7, to adjust the expected flux closer to 100 suns based on modified transmittance and reflectance values.

CASE	GEOMETRIC PARAMETER (METERS)						TRACKING ERROR (MRAD)	ENERGY INTERCEPTION FACTOR	
								SURFACE SLOPE ERROR, MRAD	
	Z_T	R_{To}	L_T	θ (DEG)	R_{Co}	R_{C1}		2	4
1	2.136	0.23	0.067	60	0.3	2.3	2	0.648	0.621
2	0.260	0.15	0.098	30	0.4	2.3	2	0.688	0.678
3	0.608	0.1	0.158	3	0.6	2.3	2	0.715	0.710
4a	0.75	0.075	0.214	1	0.6	2.3	2	0.725	
4b	0.75	0.075	0.214	1	0.6	2.3	0	0.737	

CR = 150

ENCLOSURE DIAMETER - 5.2 m

Figure 3-7: Reflector and Receiver Configuration Trades

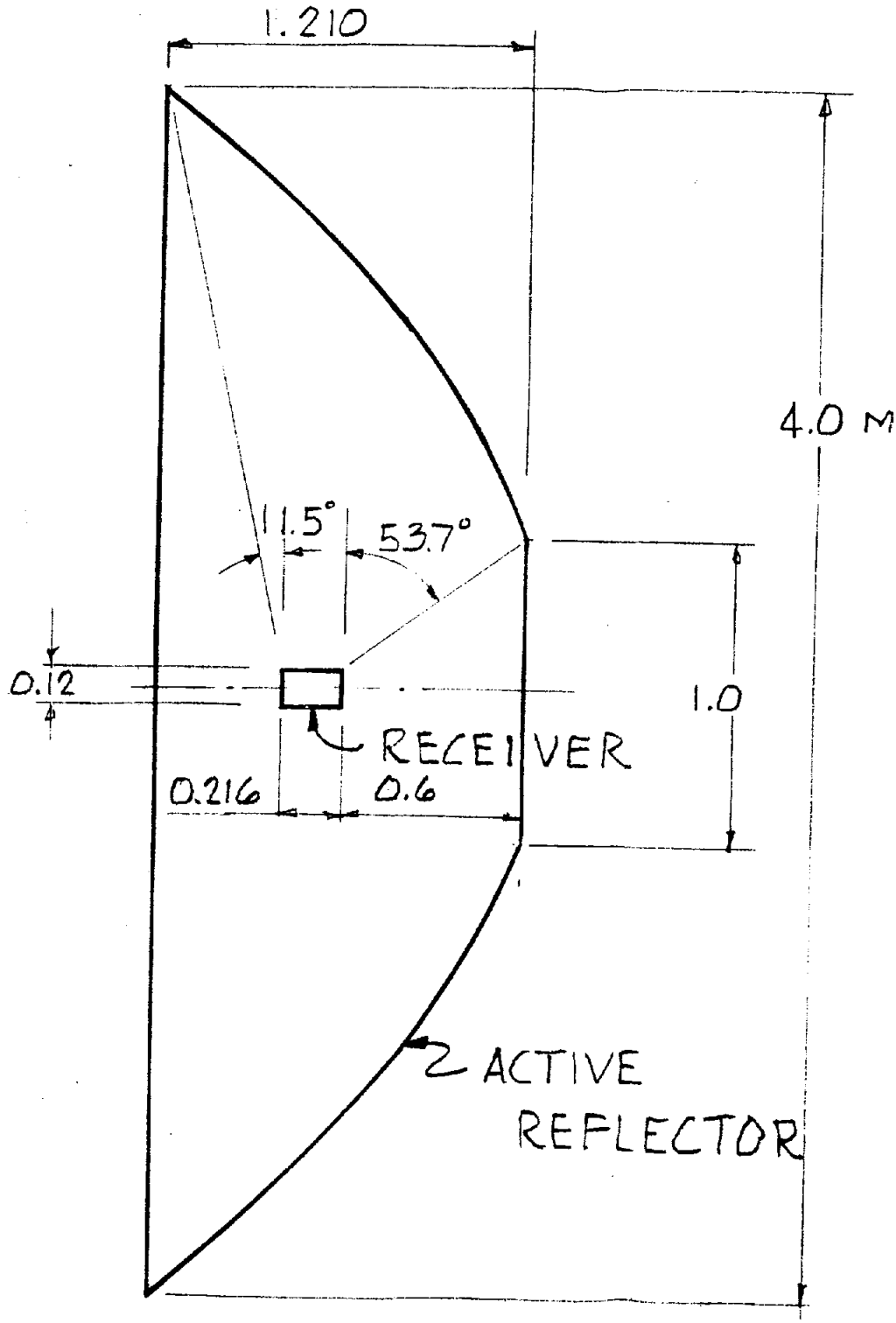

Figure 3-8: Baseline Configuration

A representative photovoltaic cell receiver concept is illustrated in Figure 3-9. This concept is based on cell sizing to achieve good cell efficiency at a nominal flux intensity of 100 suns. The cell size of 5.33 x 1.8 cm results in a yield of 3 cells per 7.62 cm diameter silicon wafer which is a standard wafer size. To meet the cell area requirements, 104 cells are arranged with a shingle overlap in the circumferential direction as shown in Figure 3-9. The cells are arranged with 4 cells in the axial direction and 26 cells in the circumferential direction. Each axial cell group is connected in parallel. The cells can be bonded to the receiver using a RTV silicon adhesive having high thermal conductivity.

3.2.3 Reflector Support Shell

Because the reflector is not subjected to wind loads, the production reflector support shell structure would be made from ultra-lightweight sandwich materials. The sandwich skin would consist of two layers of vacuum bagged 7781 style fiberglass fabric and polyester resin (.050 cm total skin thickness). The sandwich core is a 32 kg/m^3 (2 lb/ft^3) rigid urethane foam with a thickness of 2.5 cm. A rigid hollow fiberglass ring stiffener would be used at the shell rim to resist deflections due to reflector film pressure loads and gravity. Local reinforcement would be provided at the yoke bearings and photovoltaic cell array support points to sustain concentrated loads .

Average shell weight is less than 4.9 kg/m^2 (1.0 lb/ft^2) which is comparable to similar sandwich shells being built for commercial communication antenna applications (for example, by Systems Resources Co., Billerica, MA). In mass production, the shell structure costs are expected to be on the order of \$16.00 to \$21.50/m^2 (\$1.50 to \$2.00/ft^2) of shell surface.

3.2.4 Yoke, Drive and Control System

The reflector assembly is supported by a steel tube yoke which provides the gimbaling required for the azimuth-elevation sun tracking capabilities. The elevation drive is located at one of the two bearing mount interfaces between the yoke and reflector support shell. A precision rotary potentiometer is connected to the other bearing mount to provide positioning feedback to the elevation control system. The azimuth drive is located at the yoke base along

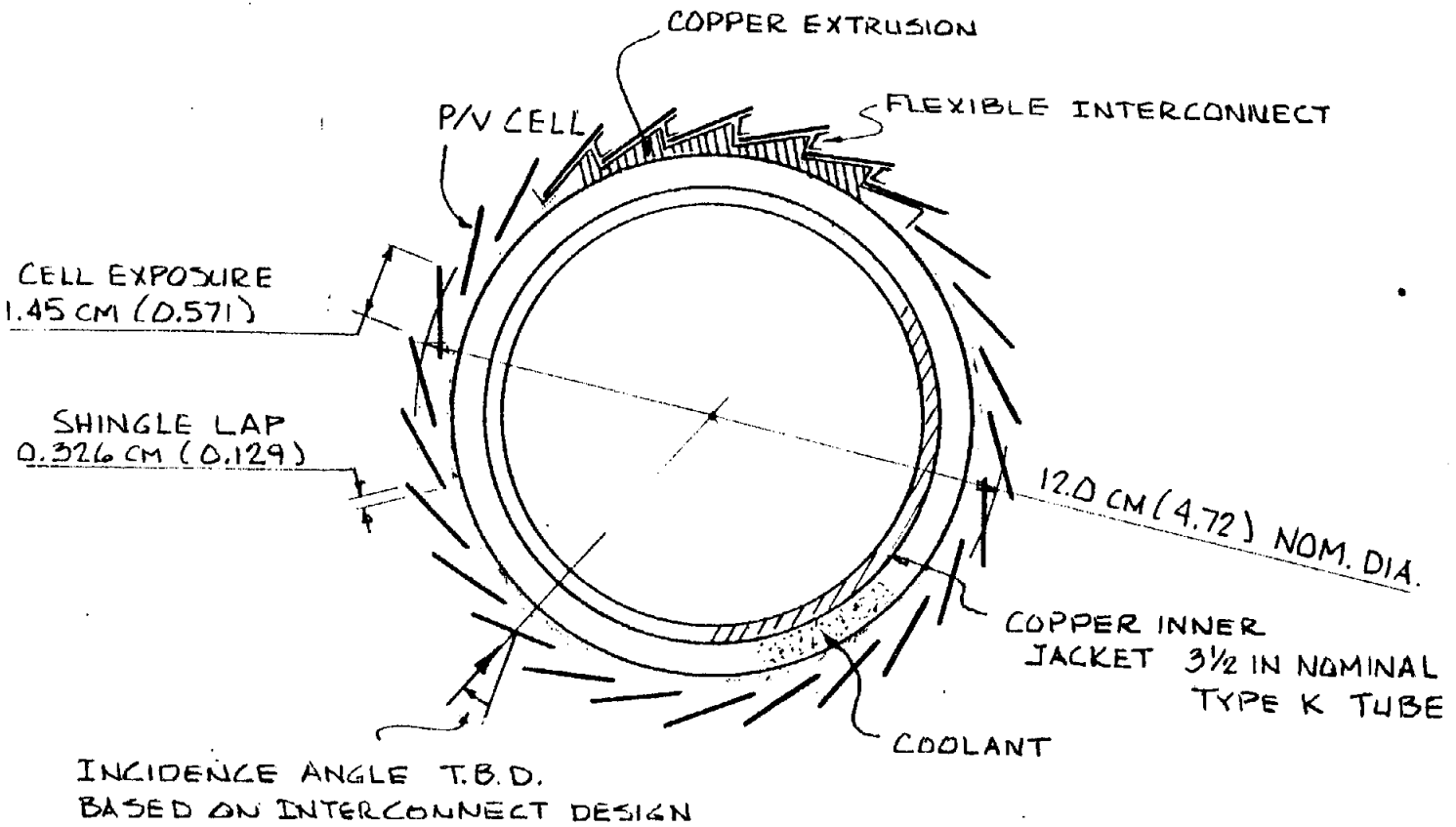

Figure 3-9: Photovoltaic Receiver Concept

with another rotary potentiometer to provide the positioning feedback to the azimuth control system. Stepper motors would be used for the drive systems because of the following reasons:

A microprocessor controller would be located at each concentrator and provide coarse tracking for sun acquisition using ephemeris data and servopots. It would also provide accurate tracking once the concentrator is on line by using two pairs of photosensors; a suitable suntracker having paired photosensors has been developed by Motorola for Sandia Laboratories. The pairs of photosensors are used for elevation and azimuth tracking in a closed-loop mode with the unit controller. The photosensor would track the sun with angular errors less than 2 mrad.

3.3 Concentrator Prototype Design Features

Some of the conceptual concentrator design features were modified on the prototype concentrator design. The reflector support shell was built using conventional fiberglass lay-up procedures and a target post was built to simulate the photovoltaic cell receiver.

3.3.1 Prototype Reflector Support Shell

A prototype reflector support shell was fabricated by a local fiberglass shop (Seattle Fiberglass Works). In the interest of keeping costs down, the prototype shell was built by a conventional fiberglass cloth layup and polyester resin spray process. The prototype shell consisted of sandwich construction; skins were two plies of 181 style fiberglass cloth and the core was 3.8 cm (1.5 inches) of rigid PVC plastic foam, commonly used in boat construction. Plywood inserts were used to stiffen the shell at the yoke bearings, as shown in Figure 3-10 and target post support points. Because of the layup process that was used, the prototype shell was excessively heavy and exhibited large gravity deflections. During testing, a cable tie on a diameter perpendicular to the elevation gimbal axis was used to suppress the gravity induced rim deflections.

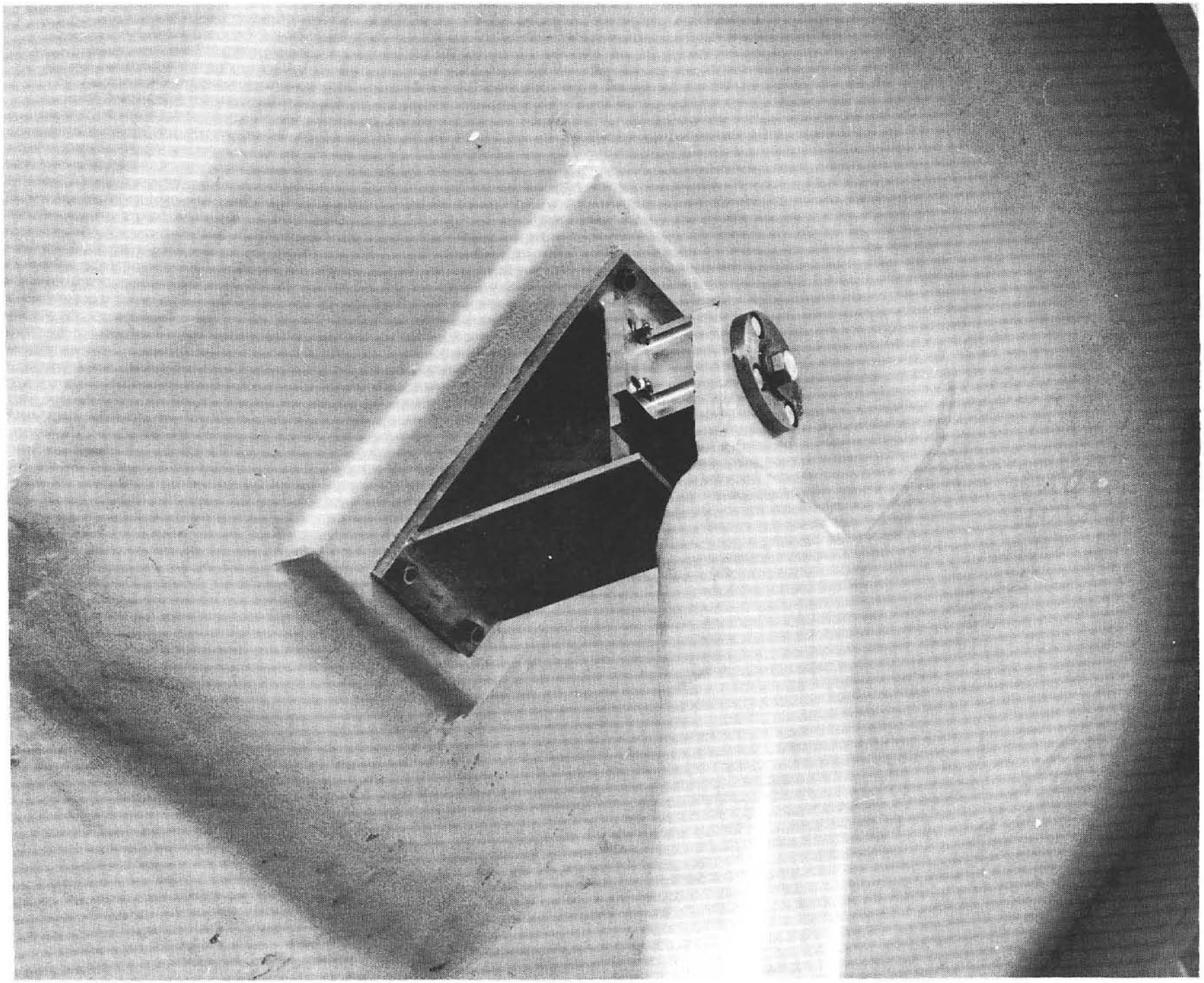

Figure 3-10: Prototype Reflector Support Shell and Yoke Bearings

3.3.2 Prototype Photovoltaic Module Target

The photovoltaic receiver, discussed in Section 3.2.2, was simulated by building a tubular aluminum target, as shown in Figure 6-2. An inner concentric aluminum tube was welded to end bulkheads with pipe fittings to form a concentric coolant passage, which would be needed for outdoor testing. Also, fittings were welded in place at the center of the target cylinder and in the end bulkhead to provide mounting surfaces for flux sensors. The target has the same mean diameter as the photovoltaic receiver; excess length was provided to allow display of the flux spill-over.

The target was attached to a thin wall steel tube mast. A spider mount scheme was used to support the target mast with adjustment provisions for alignment. For the planned outdoor testing, the mast was capable of being rotated and shifted axially to accomplish flux scanning with the flux sensor on the target surface. A flux sensor on the end bulkhead (facing the sun) would allow real time calibration of concentrated flux levels.

4.0 REFLECTOR DESIGN

4.1 Reflector Design Features

The reflector was assembled from twenty-four 15° angle gore shaped segments using .05 mm (.002 in) thick, acrylic overcoated, first surface silvered polyester film as the baseline material. While the material is not yet in production, lab samples indicate a specular reflectance of 85-90% can be achieved. Results of exposure testing of production samples using the same acrylic overcoating on aluminized polyester show improved weatherability characteristics over previous coated and uncoated metalized films. The reflector was designed to be wrinkle-free at a nominal stabilization pressure of 172 Pa (.025 psi). At this pressure level, the maximum film stress is 6.895 MPa (1000) psi and occurs in the circumferential direction at the perimeter. Based on the results of a NASTRAN computer model discussed in Section 5.2, a 15° gore configuration, which minimizes compressive seam wrinkles, was selected.

Figure 4-1 is the drawing of the reflector/reflector support shell/yoke interface. The reflector was initially attached to the support shell with two reflector mounting rings located at a radius of .45 m and 2.05 m. As discussed in Section 5.2, the inner ring was replaced on subsequent reflectors with a system that permits the reflector to free float around the target post. The prototype reflector had an effective surface radius of 2 m. The actual radius was 2.05 m which allowed the "edge roll" and wrinkles caused by attachment to the reflector support shell to dissipate without causing major disturbances of the effective reflective area.

The reflector gore joining technique that was the strongest and most durable was a 12.5 mm (0.5 in) overlap seam with double-back tape and a machine sewn stitch down the center of the seam. This provided adequate strength with no apparent long term creep at the stabilization pressure. Thermoplastic adhesives had been used previously, but problems associated with heat sealing (heat shrinking of the reflective film) caused wrinkling along the seams.

BOEING ENGINEERING & CONSTRUCTION

THE BOEING ENERGY AND ENVIRONMENT DIVISION

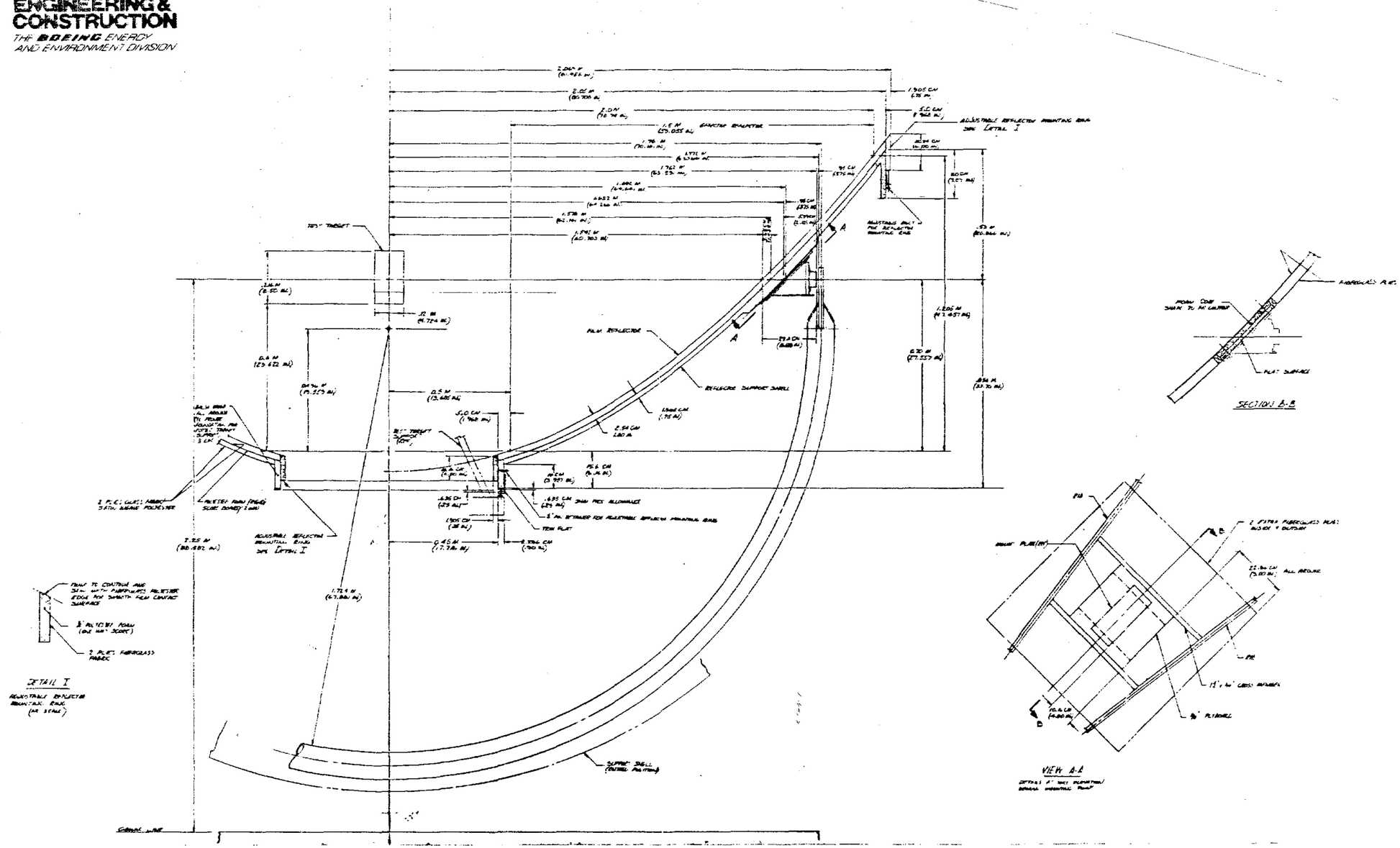

Figure 4-1: Reflector/Reflector Support Shell/Yoke Interface

4.2 Reflector Contour Analysis

A reflector contour analysis was performed to generate the reflector gore template shape and the lay-up tool contour that provided the desired flux distribution on the photovoltaic module. The basic equations used in the computer model, SEAMS, to determine the lay-up tool and gore template dimensions, were adapted from those used in the previous work on parabolic reflectors.

An approximate solution for the tool contour was found by assuming film displacements occur essentially normal to its surface. The true displacements may deviate somewhat from this assumption especially in areas with large rotations, which increase as gore size increases. For the gore geometries under construction, this effect is believed to be small.

The desired reflector contour was generated by a subroutine, MIRROR, contained within the SEAMS model. MIRROR employs a numerical integration procedure to determine the reflector contour which will provide uniform flux intensity over the photovoltaic receiver, by maintaining a constant ratio of projected concentrator area to receiver area. The reflected ray from the inner radius of the reflector strikes the lowest point of the receiver, and the intercept point moves up the receiver as the reflector radius increases. A first order differential equation is derived for an axisymmetric, modified-parabolic curve. With a design objective of uniform flux over the cylindrical photovoltaic cell receiver (having arbitrary size and location), coefficients for the differential equation are defined. The equation is then integrated over specified inner and outer radii using a variable step Runge-Kutta method. The mirror contour subroutine thus provides axisymmetric surface coordinates and slopes as a function of radial position.

Analysis in the SEAMS model is similar to the previous analysis for parabolic shapes [1], except that the MIRROR subroutine output replaces the parabolic equations.

The edge view of the gore segment is shown in Figure 4.2. For any point (d, z_d) on a plane intersecting the gore perpendicular to the gore centerline surface at (z,r):

$$\frac{r-d}{z_d-z} = \frac{dz}{dr}$$

NOTE: r,z, and dz/dr are all outputs of the MIRROR subroutine.

Using this relationship to describe a point (r_a,z_a) on the gore seam

(1) $$\frac{r-r_a}{z_a-z} = \frac{dz}{dr}$$

If the gore width angle is γ, then

(2) $$r_a = r_c \cos \gamma/2$$

Combining (1) and (2), gives an equation which relates the radius of the gore centerline point r_c, at the height z_a:

(3) $$\frac{r-r_c \cos \gamma/2}{z_a-z} = \frac{dz}{dr}$$

The relationship between r_c and z_a is also the (r,z) output of the MIRROR subroutines. Equation (3) can be solved iteratively using the MIRROR subroutines results until the equality is satisfied, which determines all the unknowns.

The length, s, of the curved line (i.e., the gore width) described by the intersection of the curved gore surface and the plane perpendicular to its surface at (r,z) can now be determined. It was shown in reference 1 that the exact length of the curved line can be calculated, but an approximate solution, assuming the curve is a circular arc, is very accurate and much easier to calculate.

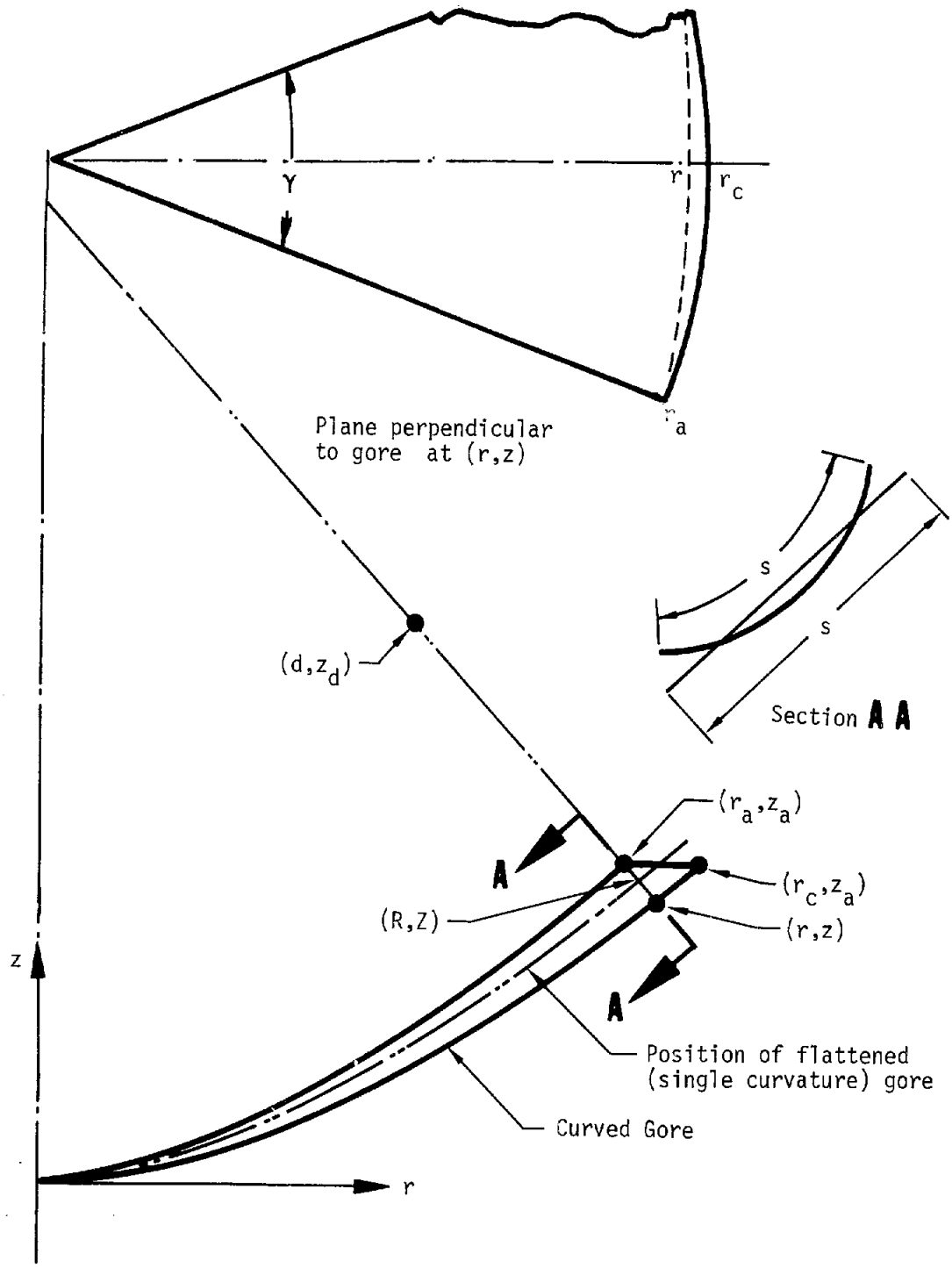

Figure 4-2: Reflector Dimensional Analysis Geometry

By straightening this line and determining the position of the resulting singly curved gore, the dimensions of the flat pattern gore and the lay-up tool in Figure 4-3 can be determined. To maintain the required gore angle, γ,

$$R = (s/2)\cot \gamma/2$$

Placing this radius on the plane through the curved line,

$$\frac{r-R}{Z-z} = \frac{dz}{dr}$$

allowing Z to be determined. Knowing the shape of the singly curved gore, its flat pattern length, ℓ, can be determined by integrating the length of the curved line described by (R,Z).

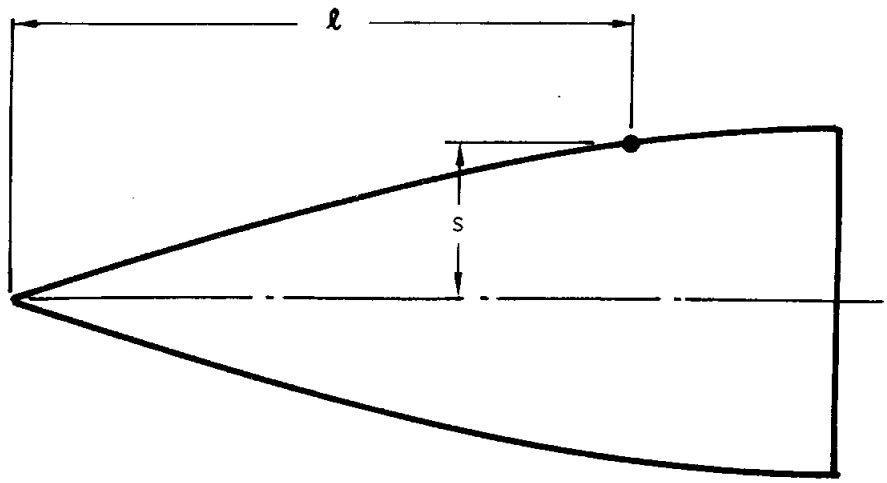

FLAT PATTERN GORE

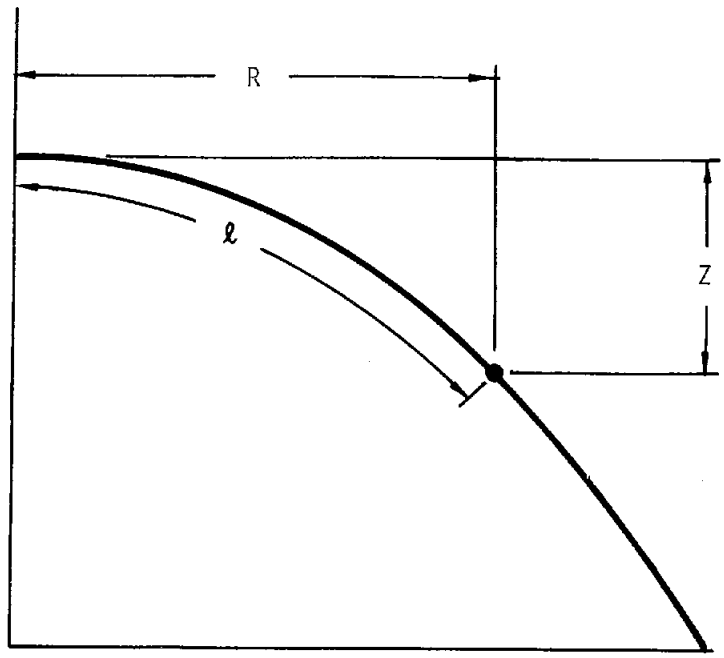

LAYUP TOOL

Figure 4-3: Gore Template and Layup Tool Dimensions

5.0 PROTOTYPE CONCENTRATOR FABRICATION

A prototype concentrator was fabricated to demonstrate and evaluate the design. The main goal was to verify the selected reflector configuration. Three 4 m diameter reflectors and two subscale 2 m diameter reflectors were fabricated and evaluated. Fabrication of more than one reflector was necessary because initial results were not satisfactory, and corrections in deficient areas were attempted.

The prototype concentrator was comprised of four major components: reflector, reflector support shell, yoke and supporting frame work, and the simulated photovoltaic receiver assembly. The following sections describe the fabrication of the reflector and the assembly of the concentrator.

5.1 Reflector Fabrication Techniques

The reflective film material used was .05 mm (.002 in) thick, first surface aluminized polyester. The polyester was metallized by National Metallizing and had a specular reflectance of 86% (0.14° cone angle). This material was selected because of its optical and mechanical properties and availability. Desert exposure testing of this material suggests that it would retain enough mechanical strength to remain operational approximately 1 to 2 years in the field.

Gore Templates

The gore templates were fabricated from 2.3 mm (.090 in) anodized aluminum in Boeing Aerospace Company's template shop. The final template was fabricated to a ±.05 mm tolerance using numerical control machinery. The templates had 1.6 mm diameter holes drilled every 15.24 cm along the edges. These holes were used to pin mark the gores during cutting and provided indexing marks for positioning of the gores during lay-up. Holes were also drilled in the template for use in indexing the attachment of the reflector to the reflector holding ring and the reflector support shell.

Table 5-1 shows the final gore template offsets versus gore centerline distance. The coordinates were the result of the analyses discussed in Section 4.2.

Using the template as shown in Figure 5-1, the gores were cut out with a scalpel. Special care was taken to avoid wrinkles in the polyester during cutting. Weights were placed on the template to avoid movement of the template during cutting.

Lay-up Tool

Shown in Figure 5-2 and 5-3 are the lay-up tools used for the construction of the 2 m and the first two 4 m diameter reflectors respectively. The lay-up tool serves as a holding fixture during tapeing of the gore seams. Accuracy of the reflector surface is established by the pre-cut gore shape and careful aligning of the gores before taping. This approach was taken to avoid the need for a highly accurate lay-up tool. The lay-up tools were constructed using supporting ribs and covered with thin sheets of cardboard or plywood. The dimensions of the supporting ribs were determined by the same computer program that provided the offsets for the gore templates. Each rib on the full scale lay-up tool had a vacuum channel which was covered with a porous tape (lawn chair webbing). This vacuum hold down system helped in maintaining gore position during taping of the seams. Figure 5-3 shows the inside of the lay-up tool with the vacuum pump and interconnecting tubing.

Reflector Gore Assembly

The gores were placed metallized side down on the lay-up tool. Using the index marks to position the gores along side of each other, the gores were butt-joined together using polyester tape. The vacuum hold-down device prevented the gores from moving once they were positioned correctly. Figure 5-4 shows the positioning of a gore on the lay-up tool before taping. Figure 5-5 shows the method used for firmly bonding the tape to the reflector film. Although there is some waviness in the polyester, the seams are wrinkle-free.

I	AGL	S	HGM
1	.00000	.00000	.00000
2	21.72099	5.71592	2.85796
3	23.90004	6.25104	3.12552
4	26.10640	6.78600	3.39300
5	28.34181	7.32081	3.66041
6	30.60784	7.85547	3.92773
7	32.90590	8.38998	4.19499
8	35.23726	8.92437	4.46218
9	37.60334	9.45862	4.72931
10	40.00425	9.99277	4.99638
11	42.44174	10.52680	5.26340
12	44.91630	11.06074	5.53037
13	47.42858	11.59459	5.79729
14	49.97914	12.12835	6.06418
15	52.56847	12.66205	6.33102
16	55.19697	13.19567	6.59784
17	57.86498	13.72924	6.86462
18	60.57275	14.26275	7.13137
19	63.32052	14.79621	7.39810
20	66.10843	15.32963	7.66481
21	68.93661	15.86300	7.93150
22	71.80512	16.39635	8.19817
23	74.71400	16.92966	8.46483
24	77.66326	17.46294	8.73147
25	80.65286	17.99620	8.99810
26	83.68274	18.52944	9.26472
27	86.75283	19.06265	9.53133
28	89.86303	19.59585	9.79793
29	93.01322	20.12903	10.06452
30	96.20325	20.66161	10.33081

Table 5-1: Gore Template Offsets (Inches)

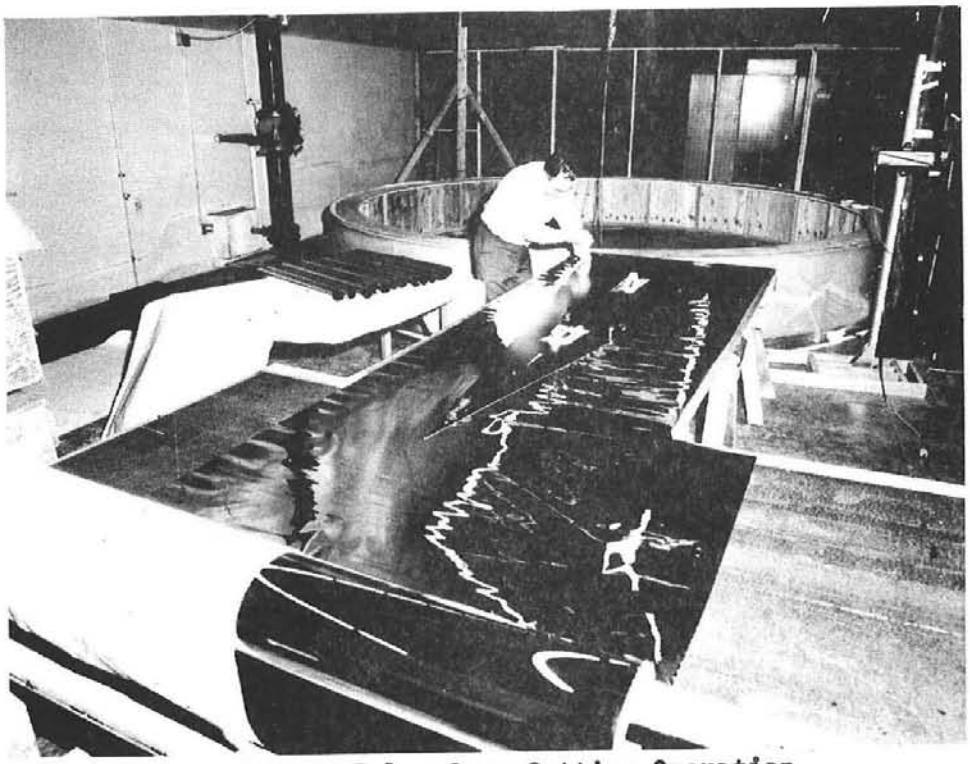

Figure 5-1: Gore Cutting Operation

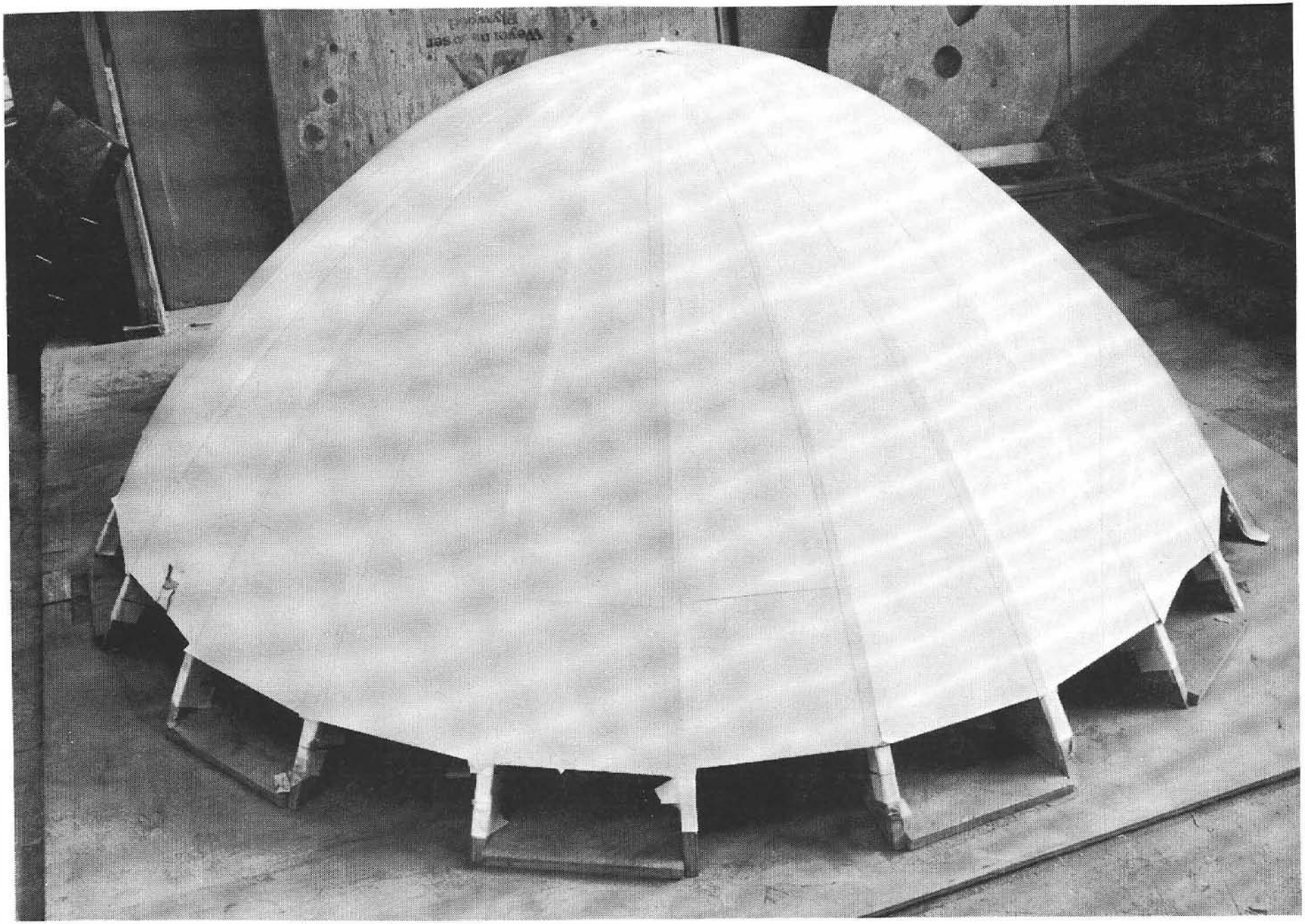

Figure 5-2: Two Meter Diameter Layup Tool

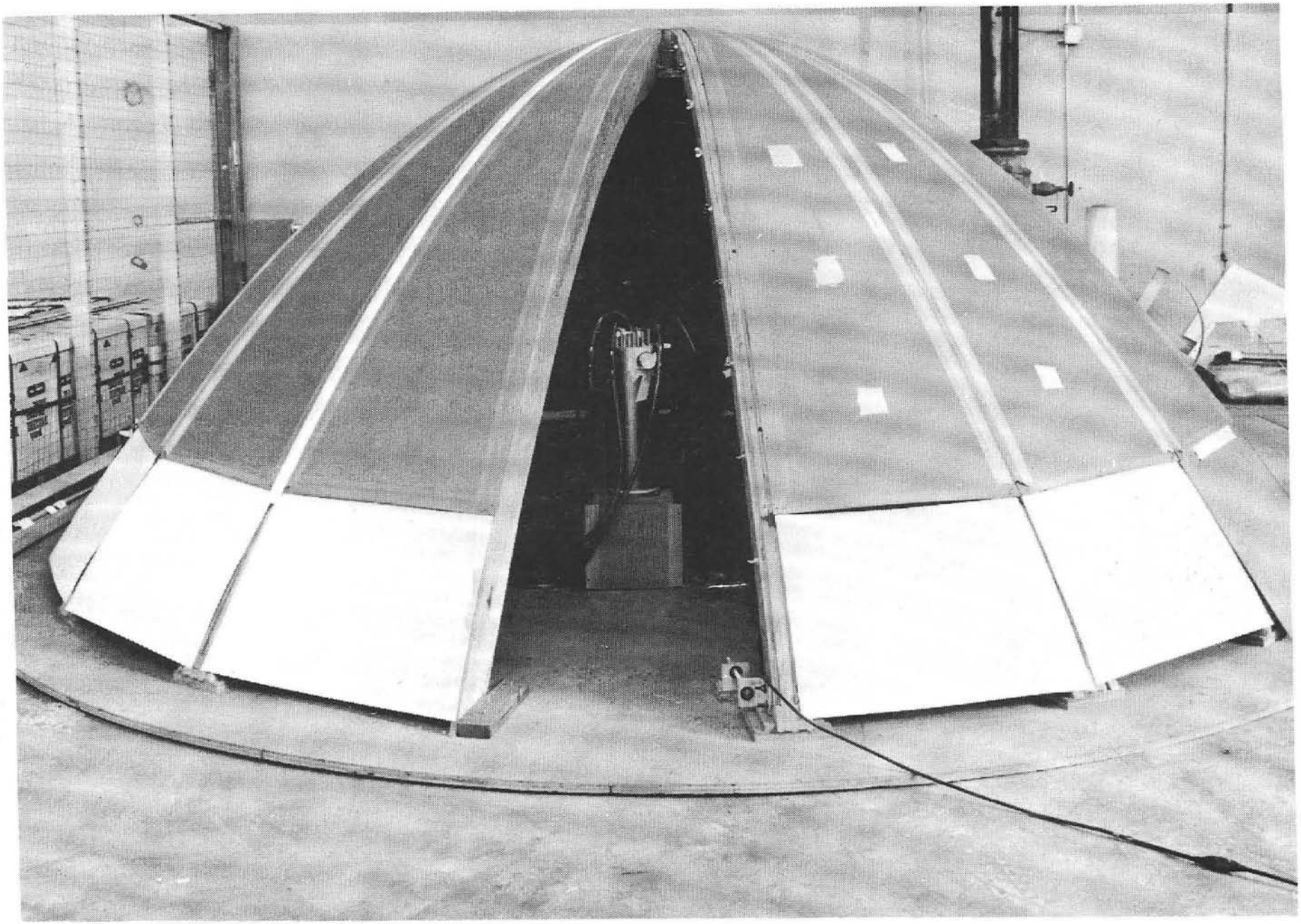

Figure 5-3: Four Meter Diameter Layup Tool

Figure 5-4: Positioning of Gore on Layup Tool

Figure 5-5: Bonding Tape to Reflector Gores

Reflector Holding Ring

A 4.57 m (15 ft) inside diameter box section wooden ring was fabricated to facilitate attaching the reflector to the reflector support shell after completion of the lay-up. Clear .127 mm thick polyester film was attached to the front side of the ring so that once the reflector was attached to the back side of the ring, it could be pressurized to its proper shape before installation.

Reflector to Reflector Support Shell Attachment

Once the gores had been joined together, the reflector was moved to the reflector support shell and placed metalized side up inside of the shell. The reflector holding ring, with the transparent polyester in place, was then lowered down over the reflector support shell by using two overhead hoists. The support shell was not attached to the yoke at this time. The reflector was then attached to the holding ring using the index marks on the gores for proper alignment. Once attached, the reflector was pressurized to its proper shape. It could now be moved back and forth, by use of the overhead hoists, in the support shell until the index marks on the gores were in alignment with the support shell. Figure 5-6 is a drawing of the reflector, attached to the reflector holding ring, being aligned in the support shell. Velcro with adhesive backing was used to attach the reflector to the shell and once attached, the reflector was taped to the shell to provide an air tight seal.

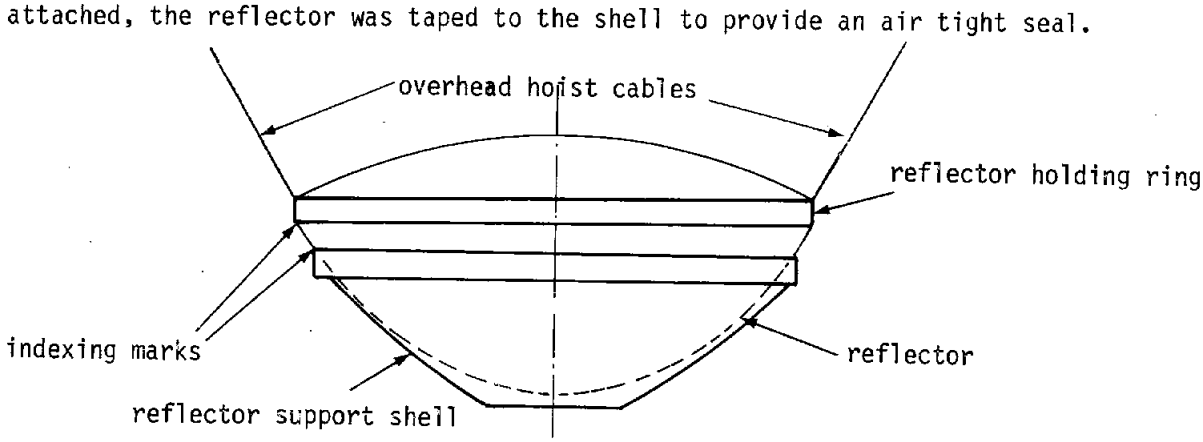

Figure 5-6: Reflector Installation and Alignment

The shell was then hoisted into position and attached to the yoke at the two bearing mounts. The target post was placed through the reflector and attached to the target post tripod.

5.2 Reflector Fabrication Results

Three 4 m diameter and two 2 m diameter reflectors were built and installed on their corresponding support shells. The first reflector constructed was a full scale prototype and was built and installed using a 20° gore angle and a gore joining technique utilizing a butt seam and 12.7 mm wide, .05 mm thick polyester tape. These techniques were developed in the previous contracts involving plastic film parabolic reflectors.

Laser scans were made and revealed this reflector to have a number of defects that would produce a non-uniform flux distribution on the photovoltaic modules. Figure 5-7 shows laser scans made of four gore centerlines. There were three major sources of errors:

1) A larger than expected "edge roll" at the outer rim (points 11-14). This was due to mounting of the reflector in a stress-free condition. Pressurized mounting would reduce this problem. In the circumferential direction, large slope errors existed in the gore-to-gore laser traces.
2) Typically, the gores have a flatter shape than ideal, which caused a circumferential dispersion of laser beams on the receiver. Variations from gore to gore in the computed flux levels were large, and in most cases, non-symmetric about the respective gore centerlines. This variation is attributed to non-uniform reflector mounting.
3) Practically all gore seams had wrinkling. These wrinkles produce beam scattering in the axial direction on the target. The dispersed beams all appeared to be incident on the receiver.

In order to understand the cause of the wrinkles (other than the result of taping inaccuracies) and define improved fabrication techniques, a NASTRAN computer model was developed for a symmetric half-gore section. Figure 5-8 shows features of the model. The model proved to be successful in predicting compression along the gore seams, boundary roll effects, and the effects of non-uniform tension during mounting. The results of the NASTRAN analysis are shown in Figure 5-9, 5-10, and 5-11. Figure 5-9 shows the gore centerline loads vs. gore angles. The load F_r is in the radial direction and the load F_o

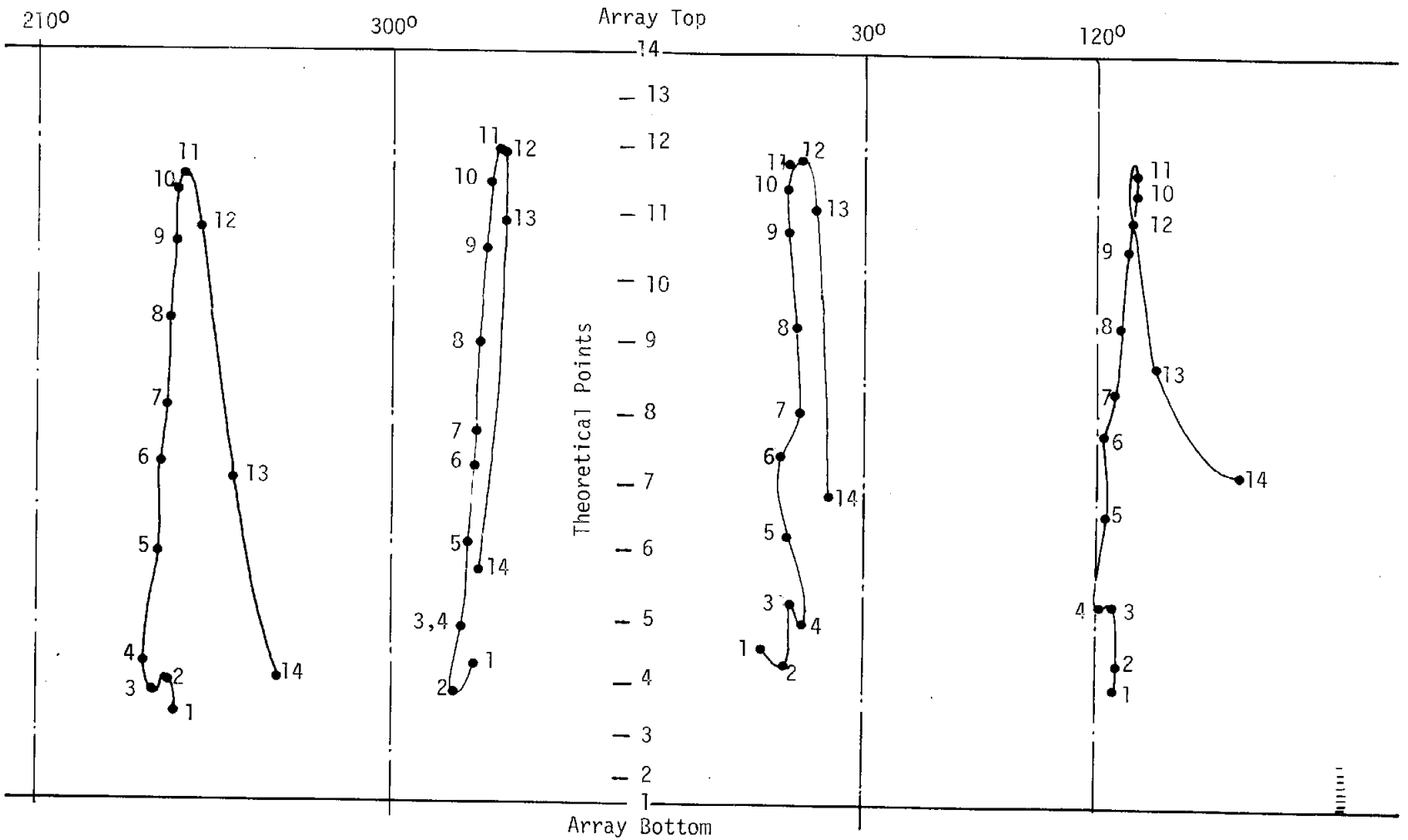

Figure 5-7: Gore Centerline Ray Traces, First Reflector

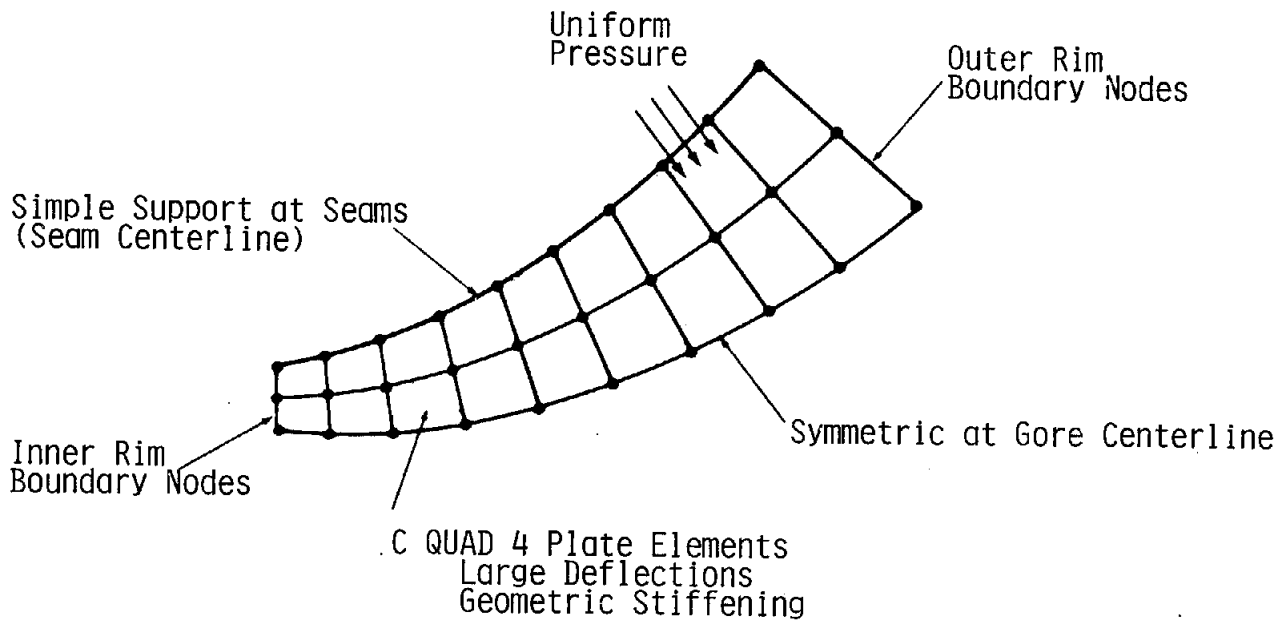

Figure 5-8: NASTRAN Finite Element Model Features

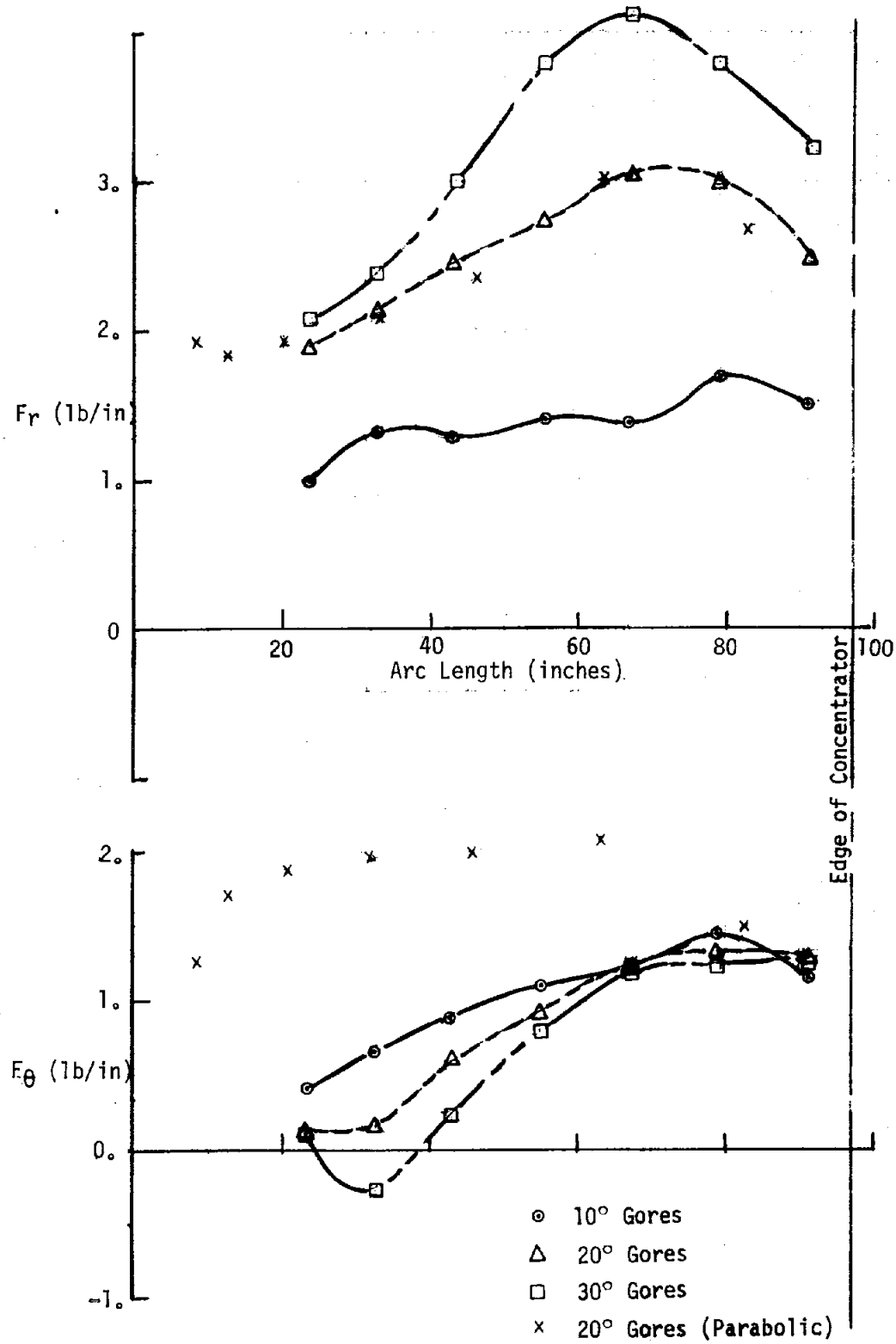

Figure 5-9: Gore Centerline Loads vs. Gore Angles

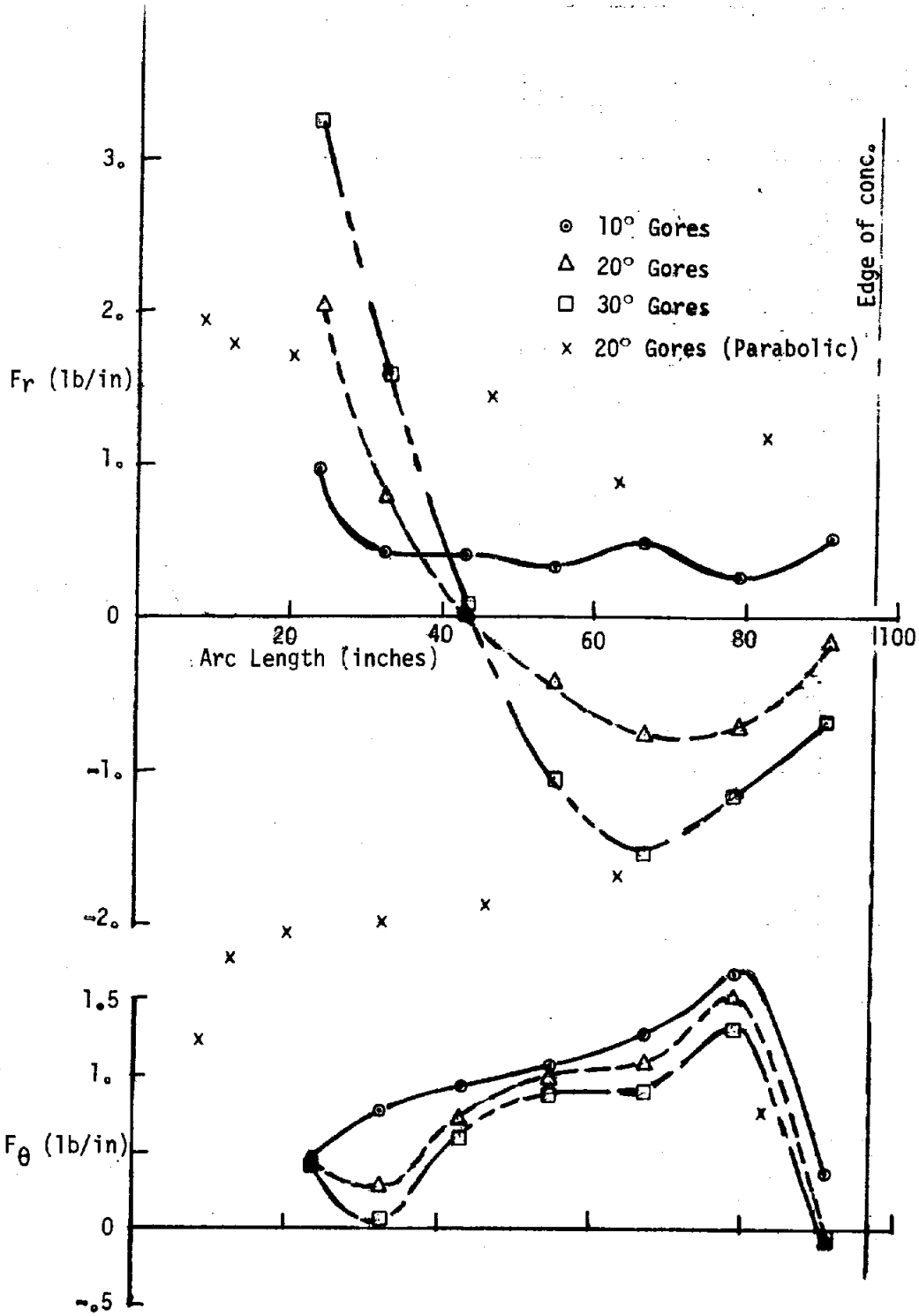

Figure 5-10: Seam Loads vs. Gore Angles

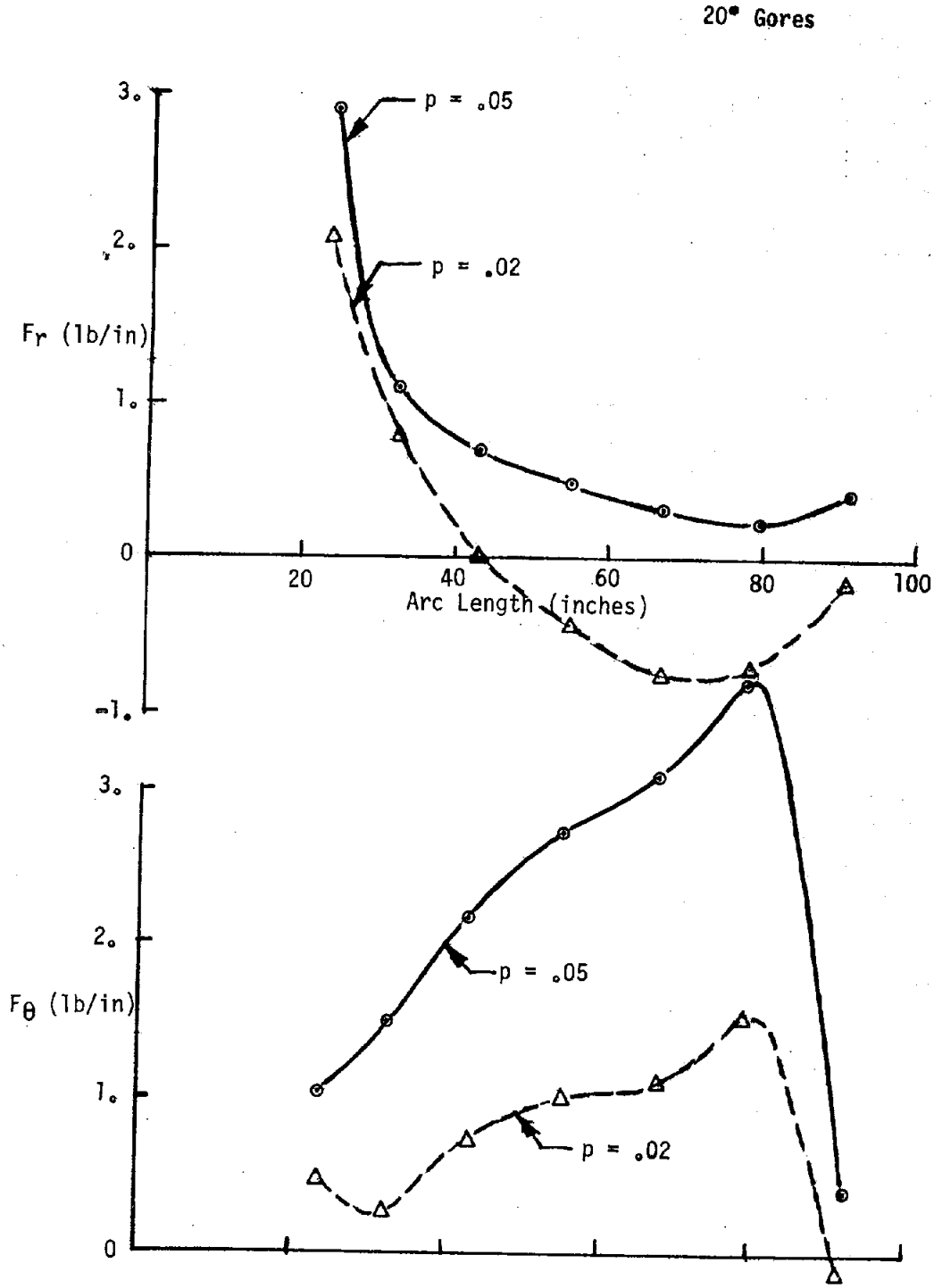

Figure 5-11: Seam Loads vs. Pressure

is in the circumferential direction. The reflector material was .05 mm (.002 in) thick, so a load of 350 N/m (2 lb/in) is equal to a film stress of 6.895 MPa (1000 psi).

Figure 5-10 are the seam loads vs. gore angles. The NASTRAN model indicated that a majority of a 20° gore angle seam was loaded compressively in the radial direction when pressurized to 138 kPa (.02 psi). A 10° gore angle seam would be in tension throughout the entire length of the seam. This indicated that a switch from a 20° gore angle to a gore of 15° or less was required to minimize compressive seam wrinkling. Figure 5-11 showed that the reflector's stabilization pressure could be raised to 172 Pa (.025 psi) while retaining a seam stress equal to the allowable of 6.895 MPa (1000 psi).

The supporting framework and yoke bearings were stiffened to compensate for the fiberglass reflector support shell being heavier than designed.

Two 2 m diameter reflectors were fabricated to verify the several improvements in the fabrication technique before construction of another full scale reflector. The gore angle was changed from 20° to 15° and various gore joining techniques and material thicknesses were tried. Visual observations verified that there were fewer wrinkles due to the gore angle reduction even though the addition of 8 more gores increased the number of wrinkles caused by taping inaccuracies.

A new method for minimizing reflector distortion caused by passing the photovoltaic module post through the reflector was tried and proved successful. The previous design, as shown in Figure 5-12, caused distortion in the reflector near the post due to circumferential misalignment of the reflector. The new method consisted of a washer with a larger inside diameter than the target posts outside diameter and was fastened to the reflector at the polar cap. When the reflector is in the support shell, the washer permits the polar cap to float freely and properly align itself around the target post. A secondary washer is installed to eliminate any air loss. Figure 5-13 shows a subscale reflector with 15° gores and an aluminized, .05 mm thick, 50 mm wide polyester tape (3M's YS-41) that was an improvement over the previously used 12.7 mm clear polyester tape. This tape was used for construction of the second full scale reflector.

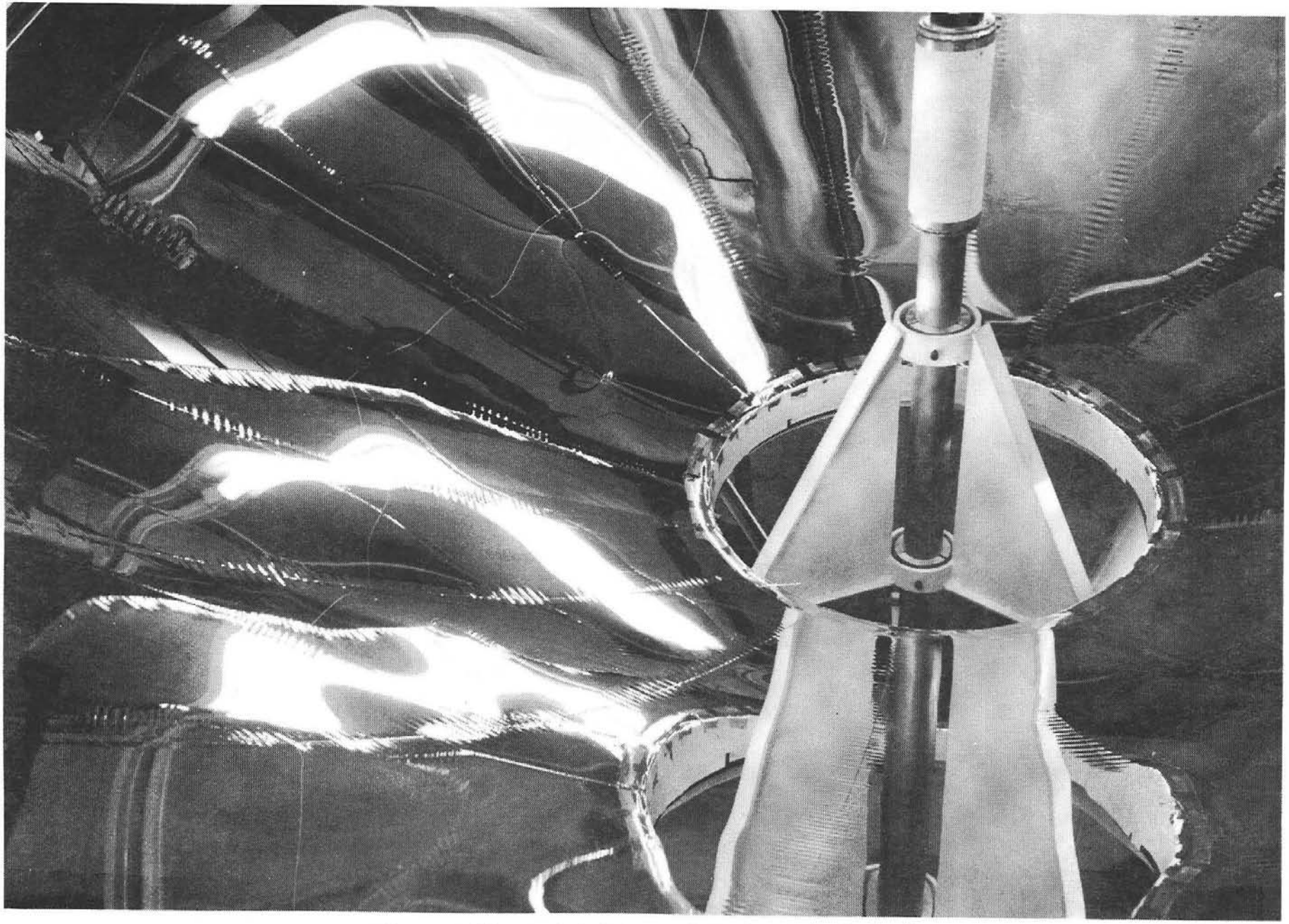

Figure 5-12: Initial Inner Attachment Method of Reflector to Reflector Support Shell

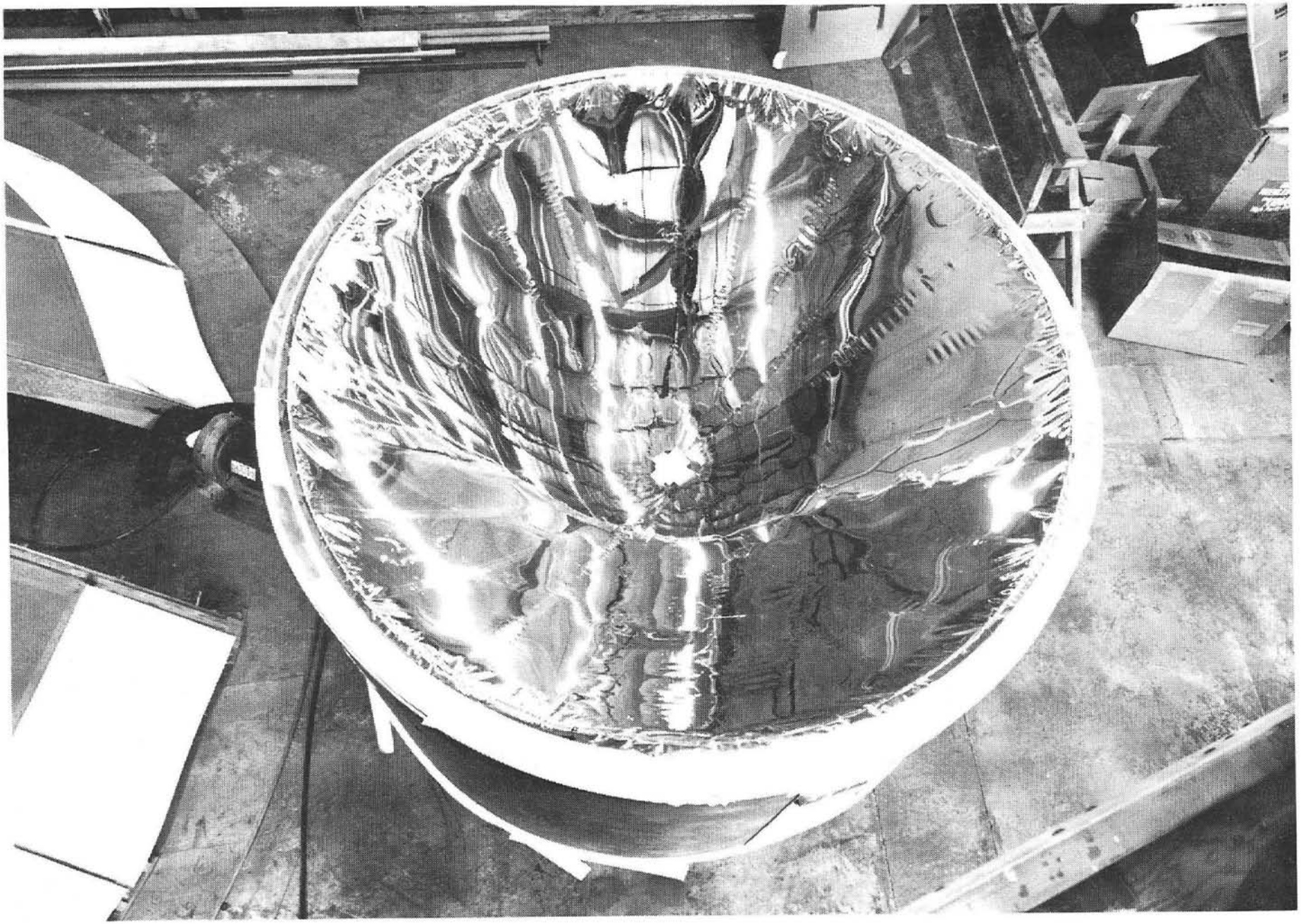

Figure 5-13: Two Meter Diameter Reflector

The second full scale reflector was then built and installed using 15° gore angles, 3M's YS-41 tape, and the reflector holding ring which permitted a pressurized mounting of the reflector to the support shell. A laser ray trace was performed on the reflector to determine its surface quality. Approximately 1300 data points were taken. Analysis of the laser ray trace showed the reflector had an intercept factor of only 0.46 based on readings along the gore centerlines. An extensive review of the computer program that determine the gore template offsets and a review of the fabrication techniques was carried out to determine why the reflector had such a low intercept factor.

Visual inspection of the mirror surface, aided by laser scanning, indicated there could be a problem with the mirror shape not directly attributable to fabrication techniques. The confidence level in the MIRROR subroutine, which generates the ideal contour, was high, so the computer code which converted the mirror contour to lay-up tool and gore template dimensions was re-examined. It was concluded that several assumptions which were based on a parabolic mirror shape, within the code, had a small but real effect on the final tooling dimensions. These assumptions were eliminated, and the rewritten code, SEAMS, was used to determine dimensions for the final reflector. This new program is described in Section 4.2. A new template was then fabricated incorporating the minor modifications.

The main cause of the low intercept factor seemed to be gore to gore seam misalignment and misalignment of the reflector in the support shell. The lay-up tool shown in Figure 5-3 that was required for the deep dish design made accurate alignment and taping of the gores difficult. In order to produce a reflector with seams aligned as accurately as possible, an alternative approach was tried.

An attempt to join gores on a flat surface which would permit closer observation and, therefore, increased gore joining precision was tried. Sample reflector gores were sent to a sail loft (North Sails, Seattle) and with close supervision, were successfully joined together with a high degree of accuracy.

Sails are constructed by joining Dacron panels together on a large, clean wooden floor. The thickness of the panels range from .076 to .203 mm depending on the desired strength characteristics of the sail. The seams are overlapping and constructed by using a double back adhesive tape (Seamstick) to correctly position the panels and then the seam is machine sewn using a zig-zag stitch. To give the sail its proper shape, the panels are cut to a predetermined curvature before joining. This curvature usually has a smaller radius than the reflector gore curvature.

The fabrication sequence used for joining the reflector gores was the same as used for joining sail panels. First one side of the doubleback tape is applied to the gore, which is pinned to the floor to prevent movement. Another gore is then carefully attached to the preceding gore. With the experience the loft personnel possess, fewer taping wrinkles along with a higher degree of accuracy was achieved in comparison to the reflectors fabricated on the lay-up tool. Once the gores were held in position by the tape, the seams were machine sewn. The gore template was built to accommodate the change from butt joining to overlap seams by adding a 12.7 mm wide strip to one side. The loft's success at joining the full scale sample gores led to a subcontract to build the third and final full scale reflector.

Creep and tensile strength tests were performed and the results showed the stitched seam to be superior to the previously used tape seams. Once completed the reflector was attached to the reflector support shell the same way the previous reflectors had been mounted (pressurized mounting, etc.). The results of the laser scans of the 3rd reflector are discussed in detail in Section 6.2.3.

5.3 Concentrator Assembly and Alignment

Once the reflector is installed in the reflector support shell, the yoke is attached to the bearing mounts on the shell. The yoke is raised until it is vertical so that the support shell rotates about the central axis. A 3.2 mm diameter cable is positioned on the support shell opposite the yoke bearing mounts to suppress the gravity deflections caused by the shell being excessively heavy. The cable is tensioned until the shell diameter becomes uniform ($4.148 \pm .003$ m).

Shown in Figure 5-14 is the method used for horizontally aligning the shell. A horizontal, rotating laser that is self aligning to an accuracy of $\pm$.05 mrad is supported by the tripod in the foreground of Figure 5-14. As the shell is rotated, the laser position on the rod (being examined in the picture) changes, indicating the amount of vertical misalignment. The shell is leveled to an accuracy of $\pm$ 3 mm. Once the shell diameter has been corrected and the shell aligned horizontally, the target post is aligned. A downward looking, self aligning ($\pm$.05 mrad) laser is supported by a traveling overhead support carriage. A smooth manual positioning system was built which minimized disturbance of the laser auto-alignment operation. The laser is used primarily for optical analysis of the reflector, but also aids in aligning the target post. The target post is placed through the reflector and supported by the target post tripod which is attached to the reflector support shell (Figure 5-16). The post is accurately positioned in the vertical direction and with the downward looking laser positioned over the center of the reflector support shell (and reflector), the target post is centered by sighting the laser through a hole drilled in the center of the top bulkhead of the post. Once the post is aligned, the concentrator is ready for optical analysis.

Figure 5-15 shows the concentrator in the vertical position, aligned and ready for testing. Figure 5-16 is a closeup of the base of the concentrator showing manometer, vacuum pump, target post tripod, and supporting framework with the elevation drive system that would be used for an outdoor test. Figures 5-17 and 5-18 illustrate the concentrator before and after pressurization. The reflector is pressurized to 172 Pa (0.025 psi) which is equivalent to a maximum film stress of 6.895 MPa (1000 psi). Also shown in Figure 5-17 is the laser and supporting carriage.

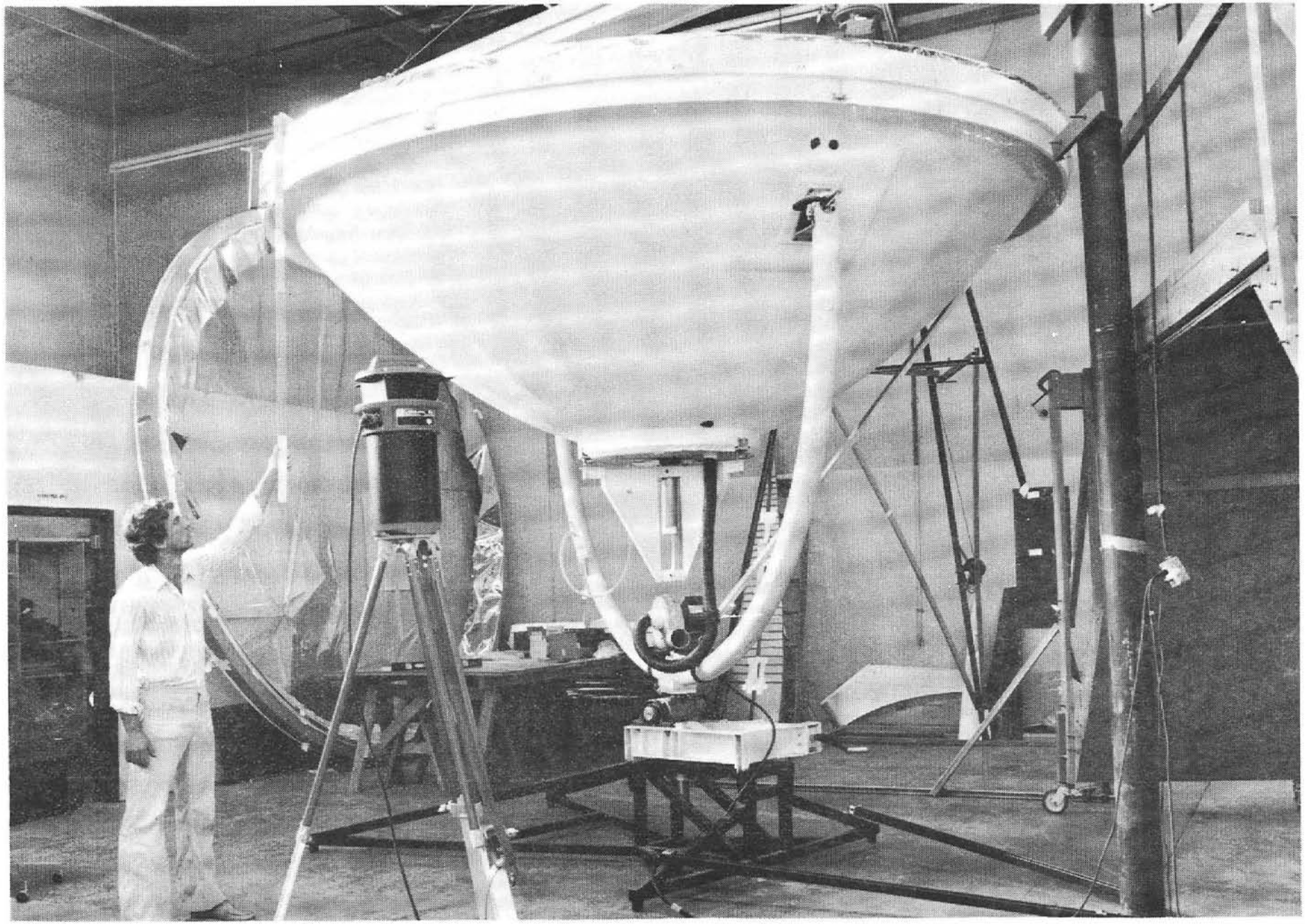

Figure 5-14: Horizontally Aligning the Reflector Support Shell

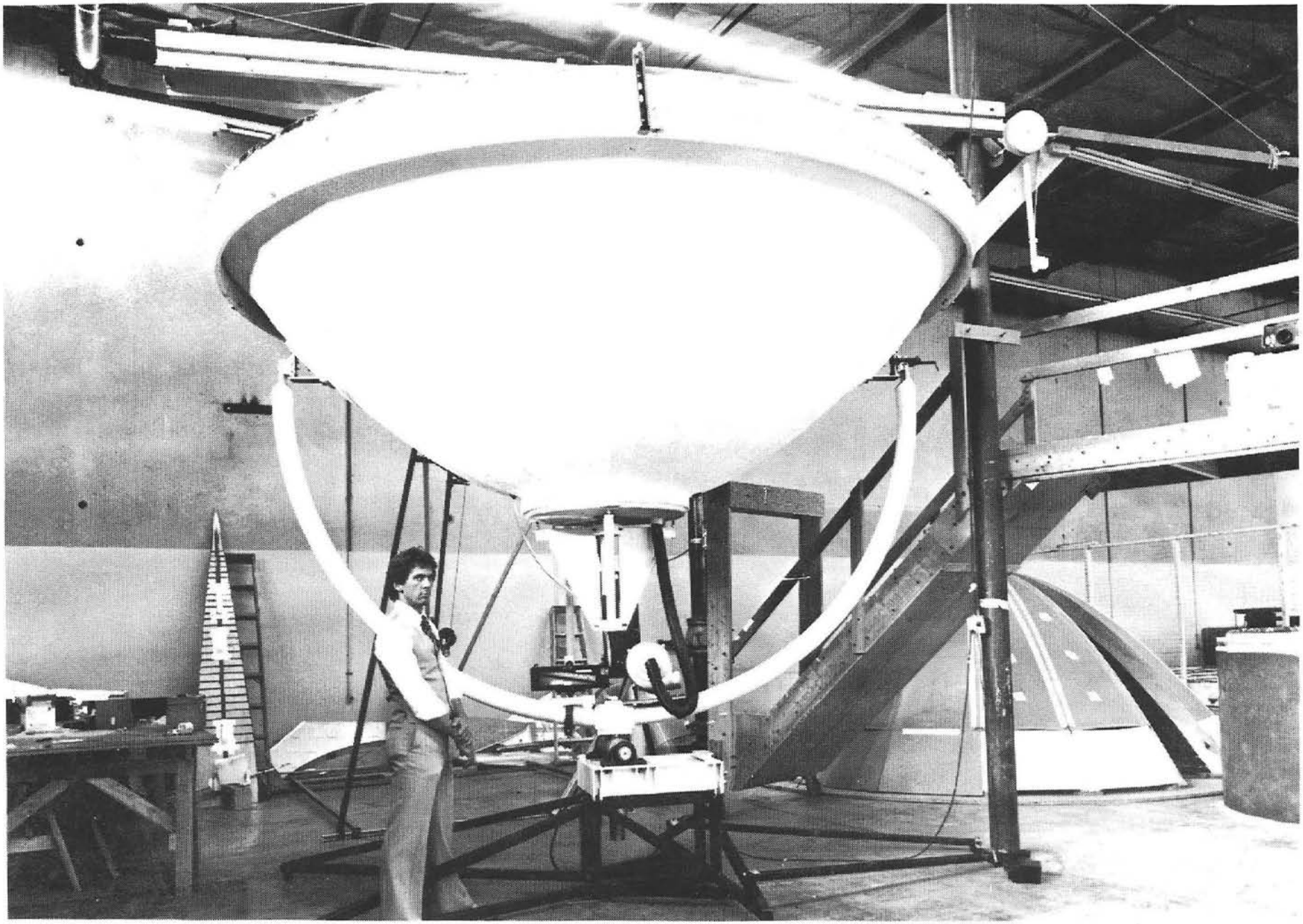

Figure 5-15: Prototype Four Meter Diameter Concentrator

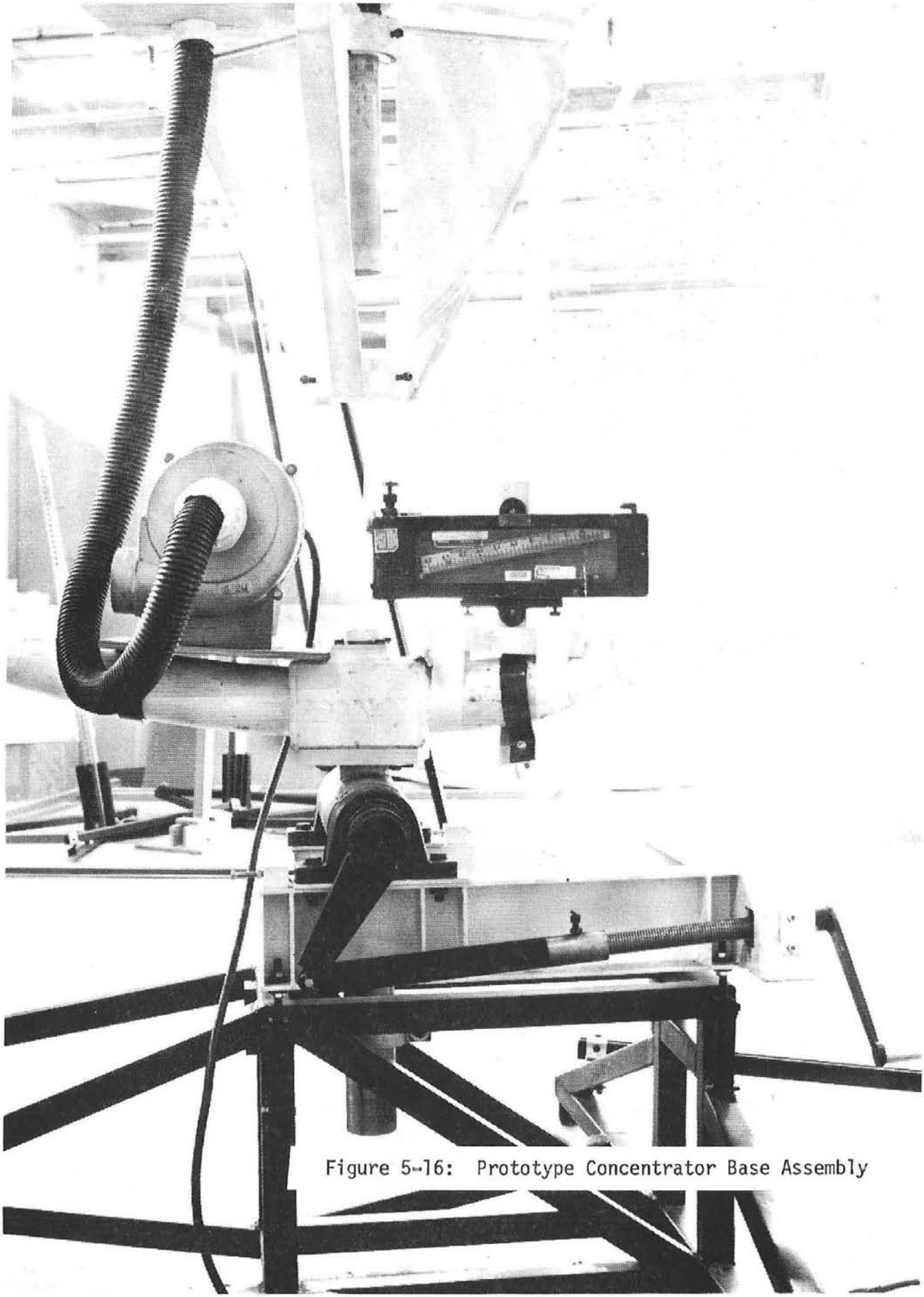

Figure 5-16: Prototype Concentrator Base Assembly

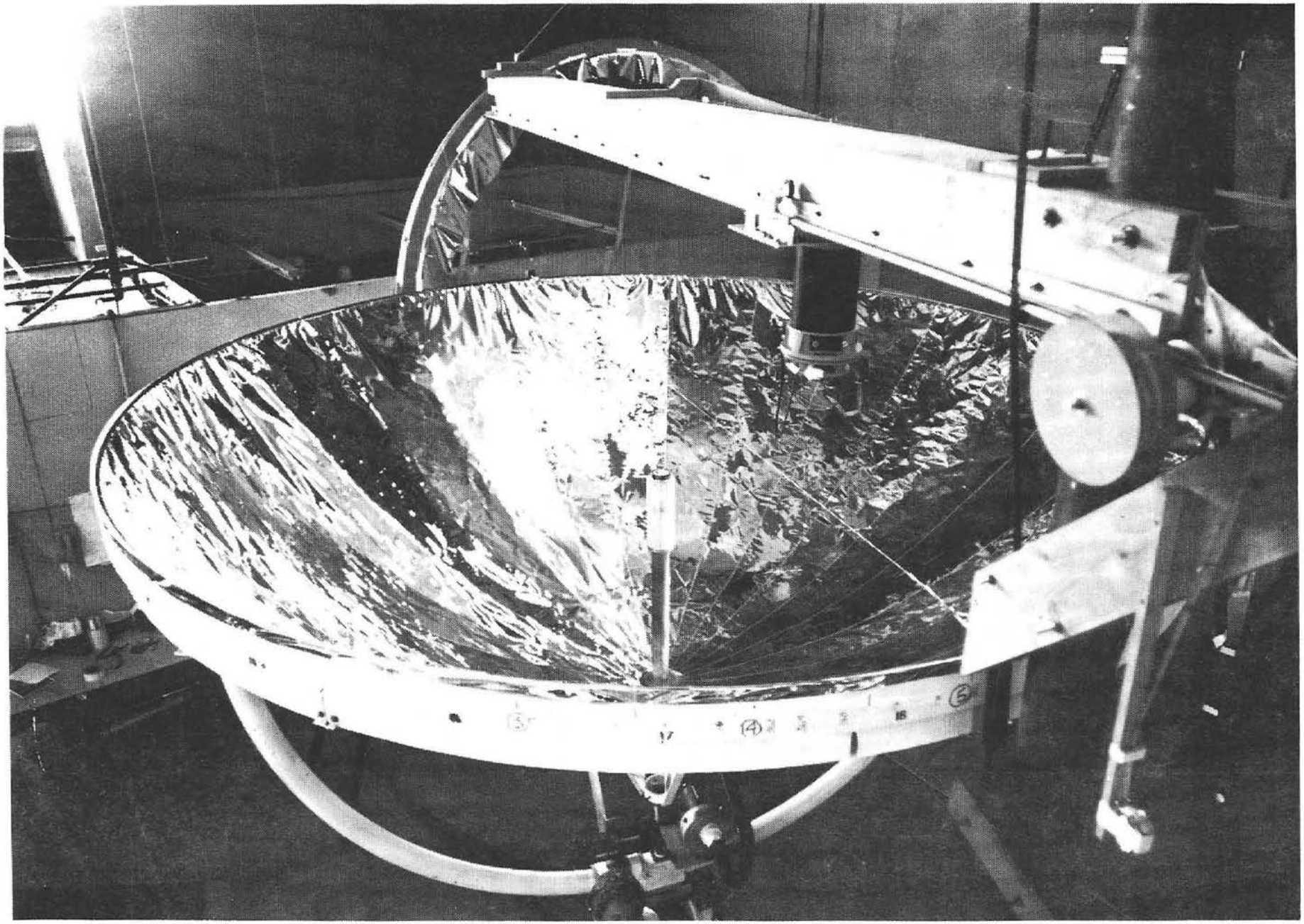

Figure 5-17: Prototype Concentrator Before Pressurization

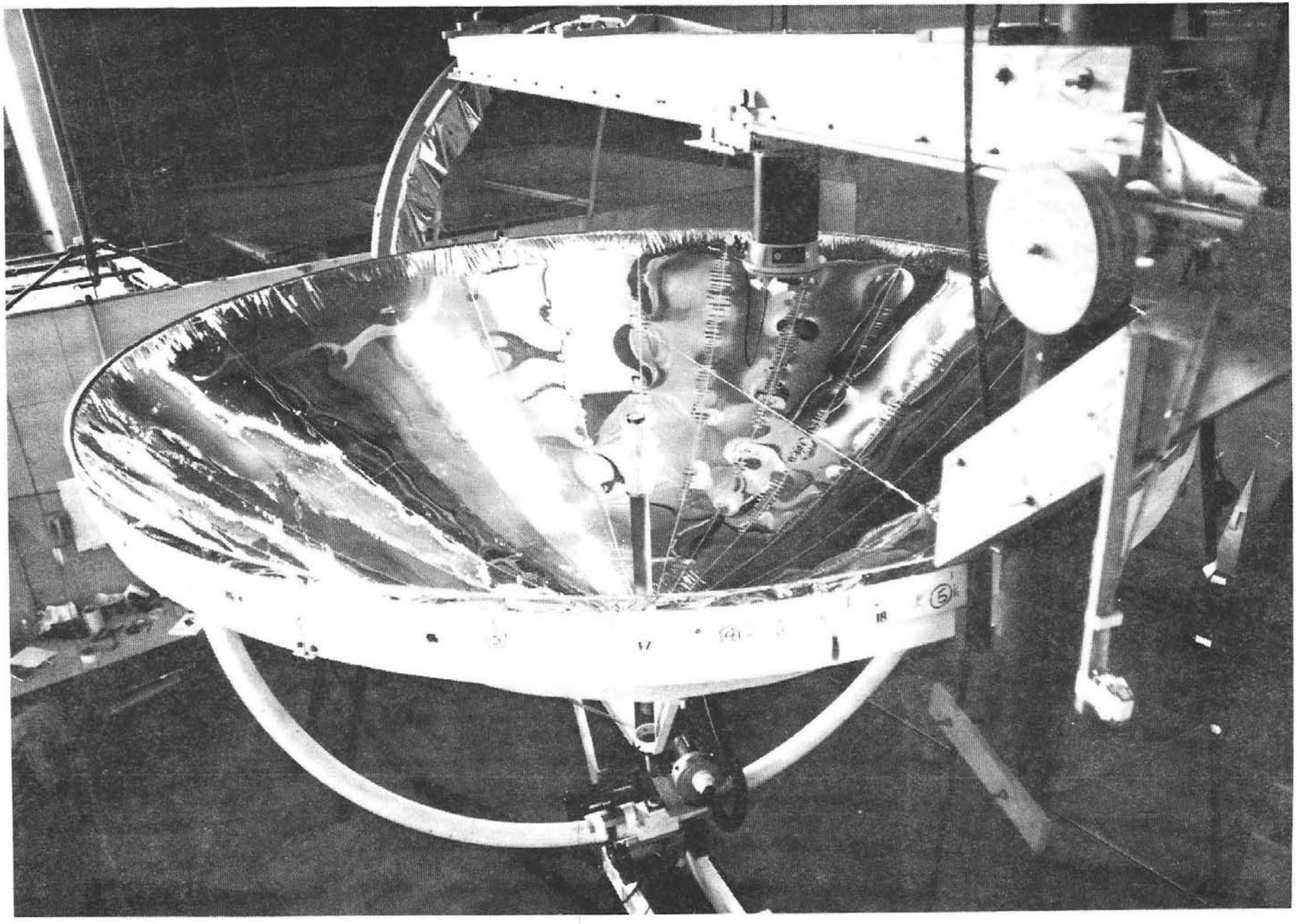

Figure 5-18: Prototype Concentrator After Pressurization (.68 Inches of Water)

6.0 PROTOTYPE CONCENTRATOR TESTING

A laser ray trace was performed on each of the three full scale reflectors to evaluate their surface errors and their ability to provide uniform flux on the simulated photovoltaic receiver. The yoke and supporting framework, shown in Figure 6-1, allowed the reflector support shell to be aligned and rotated for indoor laser ray trace testing and outdoor, real sun flux testing. The following sections describe the indoor and outdoor test procedures and the results of the laser ray trace on the third and final full scale reflector.

6.1 Outdoor Testing Plan

Provisions were made in the prototype concentrator components for outdoor, real sun flux testing with or without the enclosure. The reflector support shell, yoke, and supporting framework have the necessary bearings and pivoting capability for azimuth-elevation polar sun tracking.

As discussed in Section 3.3.2, the prototype target is water-cooled and has provisions for mounting flux sensors. By axially moving and rotating the target support tube, the flux on the cell plane can be mapped and calibrated. Also, the flux distribution can be evaluated by processing filtered photographic images with densitometer equipment. The outdoor test was not performed due to costs incurred by reflector fabrication difficulties.

6.2 Indoor Testing

6.2.1 Test Procedure

After the concentrator was aligned, a laser scan was performed on the reflector to obtain data for the surface error analysis. The testing was carried out using a Class III-B, 5 milliwatt helium-neon laser that was downward looking and self-aligning. The laser is shown in the top of Figure 5-18. The testing was performed by moving the laser horizontally on the overhead carriage to pre-determined radial positions and by rotating the concentrator to pre-determined circumferential positions.

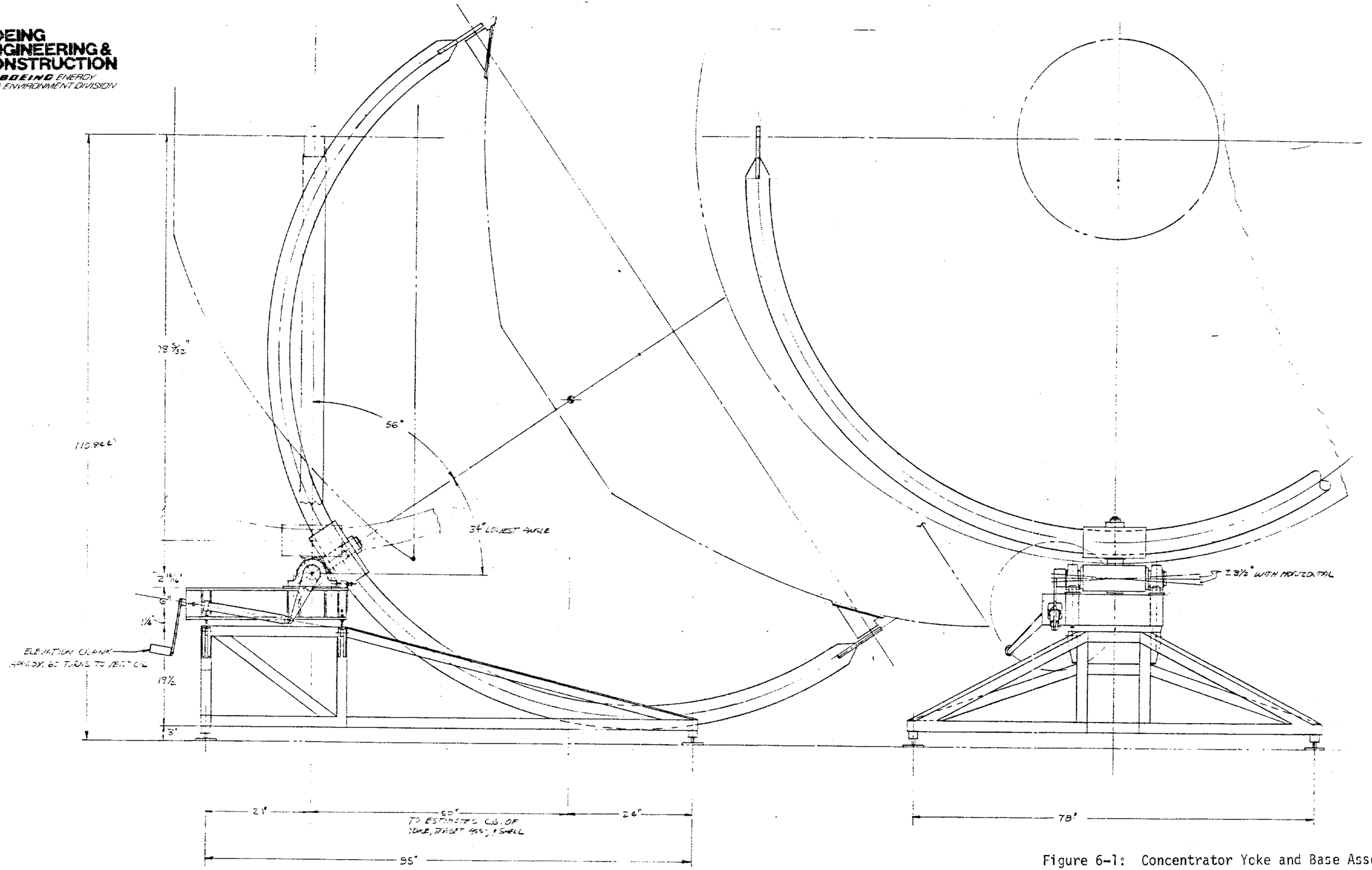

Figure 6-1: Concentrator Yoke and Base Assembly

The x-y coordinates of the laser image reflected onto the target post were recorded for use in the computer analysis. In testing the third reflector, two procedures were used. First, the gore centerlines were scanned radially every 5 cm (total of 648 data points) to determine the angular error of the centerlines. Eight consecutive gores were then scanned extensively for the purpose of flux mapping the reflected rays on the receiver. Each gore was divided into five circumferential intervals with each interval measured radially every 13 cm for a total of 480 data points for the 8 gores. The circumferential intervals were 7, 26.6, 50, 73.4 and 93% along the gore arc with each interval representative of a portion of the reflector surface. The measurements at 7 and 93% represented the reflector surface near the seams. This area had the highest slope errors due to the dispersion caused by the wrinkles at the seams. The 26.6 and 73.4% intervals represented the area between the seams and gore centerline and the 50% represented the gore centerline. The difference in represented projected areas was accounted for in the flux mapping.

6.2.2 Test Data Analysis

Surface errors of the reflector were analyzed with the aid of a computer model referred to as the ERROR code. This code allowed the analysis of a large number of laser ray trace data points and results in a description of the reflector surface in terms of:

1. overall RMS surface error,
2. overall random RMS surface error (determined by subtracting mean radial errors computed at each radius),
3. total and random surface error relative to radial position on the reflector,
4. total, radial, and circumferential surface error angle components over the entire reflector.

The following paragraphs discuss the analytical methods used in the ERROR code.

The MIRROR subroutine as described in Section 4.2 generates reflector film coordinates and slopes for the surface which will uniformly illuminate the photovoltaic target. The ERROR code transforms the test measurements to the

reflector coordinate system. Each target-hit has a corresponding reflection point on the mirror surface. A representative projected area is calculated for each target hit reflection point pair. The ideal reflected ray vector from the reflector surface to the target surface can be determined knowing the slope at the reflection point. Using the target-hit coordinates and the reflection-point, the actual reflected ray vector is calculated for each test point. The angular error (2ϵ) between the actual and ideal reflected rays can be determined from the scalar product of the two reflected ray vectors.

$$\cos 2\epsilon = \frac{\rho_A \cdot \rho_I}{|\rho_A||\rho_I|}$$

where ρ_I = ideal rays
ρ_A = actual rays

The surface error angle, ϵ, is calculated for each measurement. An overall RMS value of the ϵ angles can be found using

$$\epsilon_{rms} = \left(\frac{\sum(\epsilon^2 A_\epsilon)}{A_{total}}\right)^{1/2}$$

Where A_ϵ is the projected concentrator area corresponding to the reflection point from which was ϵ measured.

Systematic errors in the radial direction, which move the flux up an down the target plane, are removed from the test data to reveal the random surface error of the reflector. The average radial component of the error angle is calculated for concentric radial sections. The average radial error angle of each segment is subtracted from the radial component of each error angle measured in that section. When combined with the circumferential component, a RMS value for all the random surface angles can be computed.

6.2.3 Test Results

The radial centerlines of all 24 gores were scanned every 5 cm for a total of 648 data points. The RMS angular surface errors as a function of the reflector radius are shown in Figure 6-2. The overall RMS surface error was 12.95 mrad while the random RMS surface error was 7.89 mrad. The larger errors are at the inner and outer radii of the reflector. Tables 6-1, 6-2 and 6-3 show the total error angle and its radial and circumferential components, respectively. The columns are the individual gore number (1-24) and the rows (1-27) are the radial position beginning with the inside radius. The radial component tends to be the larger component of the surface error angle.

Figure 6-3 shows a laser scan from the outer radius to the inner radius along a typical gore centerline using time-lapse photography.

The results of the flux mapping of gores 1-8, shown in Tables 6-4 and 6-5, showed a nonuniform flux distribution on the simulated receiver. The target was divided into 6.5 cm^2 (1 in^2), and each data point was mapped into one of these subdivisions. The target had subdivisions the same diameter as the designed receiver; excess length was provided to allow display of the flux spillover. Table 6-4 is a "bean counting" map of the laser rays impacting the receiver. Each number represents the total of reflected laser rays that impacted that particular 6.5 cm^2 subdivision. With 100% of all reflected rays striking the target, 91.5% of the rays landed within the actual receiver boundaries. The upper and lower receiver boundaries are shown in Table 6-4 and 6-5. The first two columns and the last three represent circumferential spill-over onto the preceding and following gores.

Table 6-5 is the flux map showing the total projected area of the reflector surface associated with the target hits within each target subdivision of 6.5 cm^2. While 91.5% of the rays landed within the upper and lower receiver boundaries, these rays represented 94.5% of the reflector area. Columns 3, 4, 5, 6, and 7 have an integrated reflector projected area in the radial direction of .501, .996, .856, .623, and .353 m , respectively. In the circumferential direction, rows 4-12 have an integrated reflector projected area of .148, .336, .528, .345, .746, .419, .575, .420, and .289 m respectively.

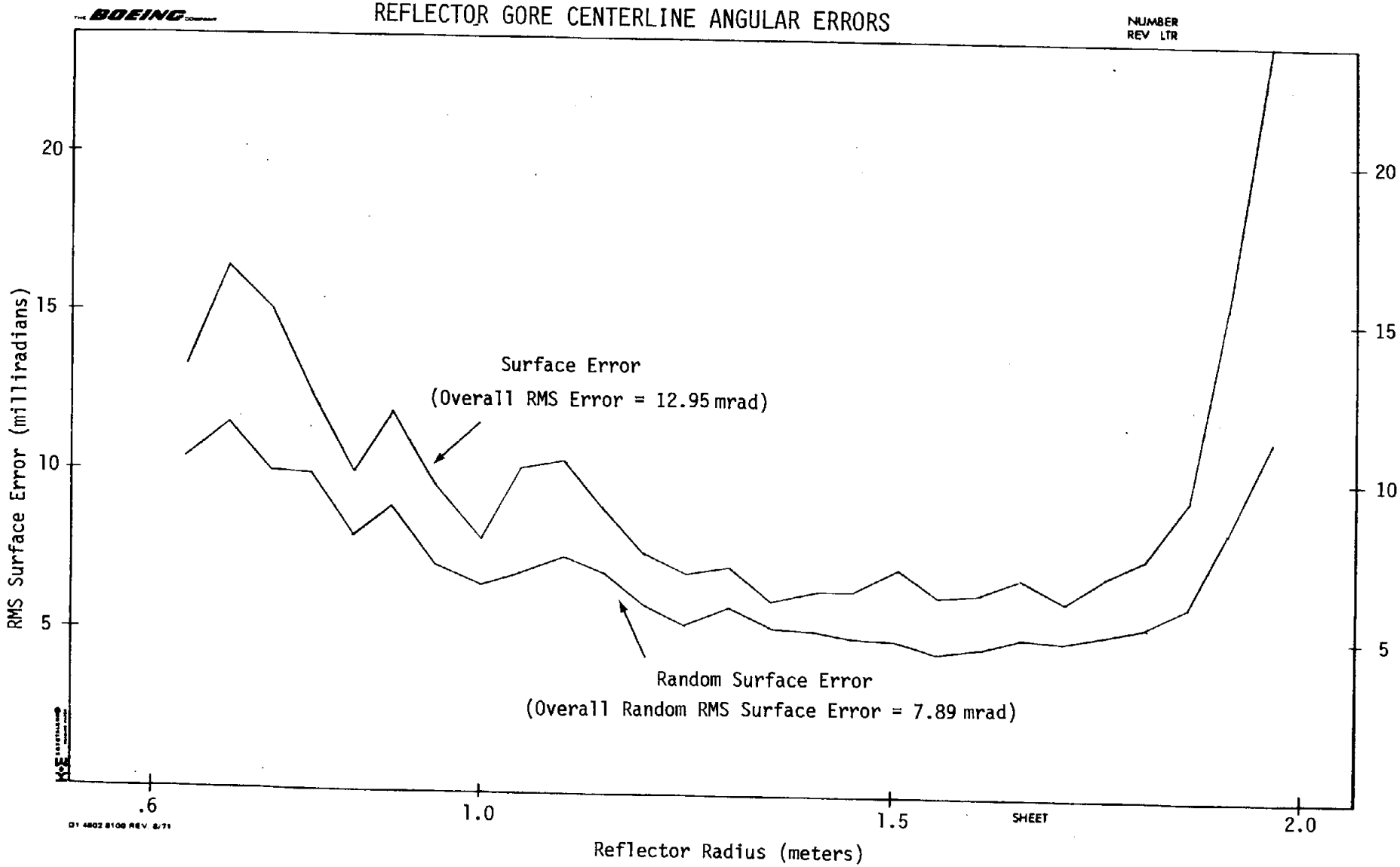

Figure 6-2: Reflector Gore Centerline Angular Errors

THESE ARE THE TOTAL ERROR ANGLES IN MILLIRADIANS

	1	2	3	4	5	6	7	8	9	10	11	12	13	14	15	16	17	18	19	20	21	22	23	24
1	31.5	16.4	15.8	18.0	10.4	11.4	6.7	10.9	11.9	7.4	7.5	6.5	4.2	12.8	3.8	12.6	7.1	4.6	9.5	10.6	12.7	19.3	8.1	22.7
2	12.7	19.4	14.5	14.2	20.3	12.4	2.4	8.9	11.3	7.4	4.0	11.6	7.7	12.2	10.7	6.7	17.8	12.6	20.4	32.8	26.6	33.8	5.8	15.1
3	16.9	4.1	27.7	15.1	23.0	17.5	9.7	9.5	5.2	4.1	11.9	7.3	11.4	7.9	9.5	13.2	17.7	10.1	12.7	18.2	19.7	30.5	5.8	19.1
4	12.9	18.3	15.9	15.9	4.9	14.2	8.3	3.8	7.5	6.7	9.2	8.1	5.1	8.6	6.5	8.6	13.4	2.3	9.1	5.1	13.1	27.9	13.6	19.2
5	7.2	17.3	15.2	1.5	6.5	7.8	7.1	3.0	4.5	7.2	6.9	8.0	8.1	8.1	2.4	4.3	6.9	11.3	7.5	9.2	19.3	10.7	17.3	9.7
6	8.1	10.8	20.0	6.3	6.5	5.9	3.4	2.7	3.9	6.7	8.6	6.8	9.8	5.7	5.6	10.3	13.9	14.7	5.8	7.8	26.9	6.7	21.8	23.9
7	9.9	11.6	4.4	2.7	8.7	4.0	6.3	4.8	5.5	9.3	4.0	6.7	17.1	4.6	5.6	5.5	13.0	11.8	5.9	5.9	12.8	3.4	19.2	22.2
8	14.8	4.7	5.9	6.1	15.2	2.8	2.2	4.7	10.0	13.2	2.4	3.6	10.4	8.1	6.4	1.1	3.7	1.3	3.4	8.4	10.8	4.7	6.5	13.3
9	7.3	19.8	14.3	5.3	15.9	6.3	4.2	10.7	9.9	8.5	2.9	9.2	11.1	8.8	6.4	1.3	7.9	5.9	8.1	11.6	12.7	11.7	10.7	12.4
10	.2	15.6	27.2	6.8	13.1	19.0	9.1	9.8	14.0	4.4	4.2	5.6	7.7	4.3	12.1	.3	8.8	5.9	6.2	6.7	5.4	12.1	16.6	16.8
11	1.3	2.6	9.2	3.0	8.7	18.5	17.8	9.3	15.5	3.2	2.6	5.3	3.0	8.5	10.5	1.7	.7	7.6	6.2	4.0	5.7	12.3	7.0	14.0
12	2.4	5.1	7.5	2.1	2.2	12.9	12.5	4.8	7.4	1.3	11.1	8.6	3.3	8.6	10.8	2.2	3.9	6.7	5.1	7.6	9.0	11.5	6.0	7.7
13	4.1	4.4	8.3	1.7	.2	8.7	6.3	11.9	7.1	11.0	10.1	4.2	1.2	1.9	4.2	7.5	4.1	7.2	4.7	8.1	10.1	4.6	10.0	3.1
14	2.9	6.0	5.3	4.7	3.8	3.2	1.2	11.5	8.0	14.4	5.8	1.1	3.3	.5	4.4	6.7	3.1	8.2	2.9	11.1	14.3	3.0	8.9	4.7
15	4.8	4.2	2.6	4.6	2.9	6.1	5.7	8.3	2.7	5.9	3.1	5.0	6.3	5.9	7.6	5.4	2.8	9.7	5.8	11.6	11.0	4.3	5.3	5.1
16	5.4	2.3	2.0	4.3	1.9	2.8	5.7	6.9	6.1	2.3	5.0	5.7	3.9	5.7	9.9	3.9	5.6	7.0	6.7	13.8	9.4	1.3	6.9	9.1
17	3.4	4.3	5.1	5.8	1.7	2.8	3.1	6.2	8.2	10.6	4.3	6.1	.7	1.4	5.3	8.7	10.9	7.0	5.0	13.5	9.7	3.8	8.9	4.9
18	7.8	7.2	6.3	1.7	.8	2.7	6.0	3.9	10.9	6.4	3.3	7.8	3.3	.8	4.2	4.9	10.8	7.7	8.6	13.9	5.6	7.9	12.3	6.8
19	9.7	8.1	7.1	.4	1.3	2.9	5.4	3.9	8.5	5.7	1.7	5.4	4.3	4.5	7.7	3.5	7.5	5.6	6.4	12.2	9.1	8.3	7.3	4.3
20	4.1	5.4	3.6	2.5	1.8	5.2	6.6	5.1	7.3	9.2	4.7	6.6	5.1	6.4	11.2	3.4	8.7	8.0	5.0	3.2	10.8	9.2	4.3	2.5
21	2.0	6.0	5.0	11.6	4.2	3.7	8.8	9.5	6.2	12.2	2.4	3.8	6.7	4.7	9.0	4.3	8.5	8.5	4.5	4.3	11.5	3.0	2.0	2.6
22	.8	3.6	3.8	9.8	6.5	7.8	4.2	9.9	1.9	9.5	6.0	3.6	3.1	8.0	11.2	4.5	8.5	4.0	2.6	2.1	7.9	3.6	1.2	4.1
23	2.2	6.8	5.8	7.8	4.0	7.0	4.1	9.4	8.4	10.0	7.4	6.4	3.3	8.2	8.5	9.0	10.5	3.0	2.6	1.9	8.2	9.3	7.2	5.8
24	5.9	4.1	9.6	6.2	1.7	7.3	5.9	8.3	8.6	8.8	4.4	3.4	3.3	11.3	8.5	9.3	6.0	3.2	3.8	6.3	8.6	10.6	10.6	12.1
25	11.7	5.7	5.6	2.9	6.9	3.1	6.4	5.0	9.7	12.4	6.1	4.3	1.8	14.1	1.8	11.9	9.9	3.0	6.9	12.5	16.0	14.1	11.0	15.2
26	19.3	15.4	1.9	3.7	13.5	6.3	5.9	6.1	11.5	14.3	9.6	9.0	15.9	19.9	7.2	14.2	19.5	13.0	26.7	26.0	22.1	16.1	15.6	21.4
27	28.0	26.3	9.5	13.5	21.0	14.6	10.9	11.1	17.8	23.6	24.7	23.6	29.8	33.1	25.5	29.3	37.4	33.1	51.6	51.6	36.7	23.5	24.7	32.3

Table 6-1: Total Gore Centerline Error Angles

THESE ARE THE RADIAL COMPONENTS OF THE ERROR ANGLES

	1	2	3	4	5	6	7	8	9	10	11	12	13	14	15	16	17	18	19	20	21	22	23	24
1	15.3	7.9	.3	6.4	3.8	5.5	3.5	2.0	1.2	1.7	3.0	2.9	1.9	6.4	1.9	4.6	1.8	1.9	3.4	2.0	2.3	1.6	.4	9.9
2	7.0	6.3	4.2	5.8	11.1	7.0	1.2	1.5	.2	3.8	1.5	4.1	3.8	6.2	5.7	3.9	9.1	7.0	9.2	17.9	14.6	12.8	3.2	7.3
3	11.0	1.5	14.8	8.4	13.9	10.7	5.9	4.2	2.2	2.3	7.7	4.5	1.5	2.8	5.9	7.9	10.6	5.8	6.2	10.5	12.0	8.1	2.2	4.1
4	9.1	4.2	7.3	9.4	2.6	7.7	4.9	4.9	5.0	4.2	6.4	5.6	2.3	4.9	4.2	5.8	8.8	1.1	.3	2.6	3.3	2.1	3.3	12.9
5	5.0	11.0	9.9	5.2	3.8	2.7	4.6	2.1	2.1	3.7	1.0	.0	2.7	5.8	.5	2.3	.1	1.3	5.0	5.1	11.3	6.1	1.9	6.8
6	4.7	6.4	15.9	.7	.8	3.4	1.3	1.3	1.5	1.7	2.7	1.7	1.6	2.5	3.4	8.1	10.2	7.8	4.3	6.1	19.0	5.2	7.4	14.9
7	7.7	7.8	3.6	2.2	.8	3.1	4.6	.8	3.6	5.7	1.1	3.7	4.9	.8	4.5	4.5	10.5	8.6	4.6	4.6	5.3	2.6	5.5	16.1
8	5.7	1.9	4.9	4.9	6.7	1.0	1.9	1.0	7.0	11.3	2.0	2.9	8.9	1.3	4.9	.9	3.0	1.1	1.0	4.1	4.4	3.9	1.1	6.0
9	.4	16.9	12.3	4.6	7.3	4.5	3.0	7.3	3.8	7.4	2.3	7.4	9.5	3.6	.5	.7	6.5	4.6	5.4	9.5	8.8	9.5	9.4	7.8
10	.2	13.8	17.6	6.1	8.6	15.4	8.1	8.0	1.9	3.1	3.2	3.9	6.9	2.9	9.9	.2	5.9	4.1	.0	5.9	3.9	7.3	15.2	14.3
11	.3	1.7	5.4	2.7	9.5	14.9	16.3	8.6	5.4	2.7	1.4	4.4	1.4	5.4	9.5	1.3	.7	5.5	1.5	.4	4.4	3.1	6.4	12.6
12	1.1	.2	2.7	1.1	.9	10.5	11.7	3.9	4.2	.9	9.2	8.1	2.1	6.7	9.7	1.9	3.1	.3	1.8	2.7	6.3	4.6	2.2	7.1
13	.0	2.0	9.8	.1	.1	3.8	5.9	3.4	6.9	9.9	8.9	3.9	.9	1.1	4.0	6.9	.0	3.1	2.9	2.1	7.1	2.0	3.6	2.9
14	.1	5.7	2.8	.1	3.7	.9	.1	3.2	7.7	13.6	5.7	.1	1.8	.1	.9	5.9	.9	3.9	2.8	4.1	11.8	2.8	3.8	4.0
15	.9	.9	.9	1.0	2.8	5.7	5.7	1.1	.9	5.7	1.0	1.0	5.7	4.7	2.9	3.8	2.8	6.7	5.7	5.9	5.9	3.7	1.9	.0
16	2.9	.8	1.9	.1	.8	.1	5.7	.7	.8	1.9	1.7	.8	2.9	5.7	8.5	3.8	4.7	5.7	6.6	12.3	3.0	.9	6.6	7.6
17	2.1	4.0	3.1	4.0	.3	.3	3.0	2.3	3.2	10.5	2.2	4.9	.3	.3	4.9	8.5	9.4	6.7	4.9	13.0	5.8	1.3	7.6	4.9
18	1.7	6.0	4.2	1.6	.2	.7	6.0	.7	6.2	6.3	3.3	7.7	3.3	.7	3.7	3.3	9.5	7.7	7.7	13.9	5.1	6.0	9.5	6.0
19	9.6	7.1	5.4	.3	1.2	1.4	5.4	3.7	3.1	5.6	.3	5.4	3.7	3.9	5.6	.5	6.2	4.5	4.5	12.2	8.8	7.9	2.9	3.7
20	4.1	.0	.0	2.5	1.6	4.9	6.6	4.1	5.7	9.0	2.4	6.6	4.1	5.7	9.0	3.3	6.5	7.4	2.4	1.6	10.6	9.0	.8	2.5
21	1.3	.5	5.0	11.4	4.2	1.8	8.4	8.4	5.8	12.2	.5	3.7	6.1	1.9	2.7	4.2	3.6	7.6	2.9	.5	10.8	2.9	1.0	1.8
22	.5	.3	2.6	8.7	6.4	5.7	2.7	8.3	1.8	8.7	5.8	3.5	1.2	1.9	5.6	4.3	4.1	2.7	2.6	1.1	6.5	2.7	1.2	.3
23	.3	6.2	4.7	6.5	4.0	4.8	2.6	6.9	4.8	7.0	7.0	6.3	2.6	.5	4.1	8.5	6.8	1.2	1.8	.3	7.0	8.4	7.0	4.8
24	4.7	3.1	9.4	5.9	1.6	5.2	1.1	6.7	1.2	.9	3.3	3.3	2.6	5.7	6.7	8.9	4.7	1.6	3.3	6.1	8.2	9.5	10.3	11.7
25	10.7	4.0	5.4	1.4	6.7	1.4	1.5	1.9	6.5	10.6	5.4	4.0	1.3	8.0	.7	11.4	9.4	1.3	6.7	12.1	15.4	13.4	10.8	14.7
26	17.9	12.6	1.8	2.7	13.0	6.0	3.3	3.3	10.4	13.6	9.2	8.6	4.8	16.0	6.6	13.7	18.7	12.4	25.6	25.0	21.2	15.6	14.9	21.6
27	26.4	23.5	9.1	11.2	20.0	14.0	9.1	10.3	17.0	22.4	23.6	22.3	28.3	29.0	24.1	27.6	35.2	31.1	48.0	48.0	34.7	22.4	23.6	33.6

Table 6-2: Gore Centerline Error Angles, Radial Components

THESE ARE THE CIRCUMFERENTIAL COMPONENTS OF THE ERROR ANGLES

	1	2	3	4	5	6	7	8	9	10	11	12	13	14	15	16	17	18	19	20	21	22	23	24
1	16.5	9.2	15.8	14.4	8.3	6.8	3.4	10.4	11.7	6.8	5.6	4.2	2.7	6.6	1.9	13.0	6.4	3.3	7.6	10.1	12.2	19.2	8.0	14.9
2	6.2	17.[illegible]	13.[illegible]	1[illegible].9	9.7	5.3	1.5	8.6	11.3	4.4	3.2	9.7	5.0	7.1	5.9	2.9	10.3	5.9	14.3	14.9	12.1	27.0	2.9	9.8
3	6.1	3.5	16.4	8.5	9.3	7.2	4.4	7.2	4.0	2.3	4.2	3.0	11.2	6.8	3.5	5.7	7.8	5.4	8.7	9.3	7.9	28.1	4.8	8.2
4	3.9	17.3	12.3	8.0	3.3	9.2	4.5	3.6	2.4	3.2	2.8	2.8	4.0	5.4	2.7	2.8	5.1	1.8	9.1	3.6	12.3	27.7	12.8	8.2
5	3.2	9.9	8.2	8.0	4.1	7.0	3.5	.9	3.6	5.3	6.8	8.0	7.3	2.9	2.3	3.1	6.9	11.1	3.8	6.3	12.5	7.2	17.1	4.0
6	5.4	7.2	4.3	6.2	6.4	4.1	3.0	2.2	3.5	6.3	7.9	6.5	9.6	4.7	3.7	2.7	6.1	11.0	2.4	1.9	13.6	1.9	19.8	8.4
7	3.3	7.[illegible]	1.0	.7	8.7	1.5	3.7	4.7	3.4	5.2	3.8	5.1	8.1	4.5	1.3	1.0	3.5	5.8	2.3	2.3	11.1	1.4	18.1	10.1
8	13.3	4.1	1.1	1.9	13.[illegible]	2.5	.4	4.5	5.8	3.9	.4	1.5	1.7	8.0	3.0	.2	1.3	.3	3.2	6.9	9.5	1.4	6.4	11.3
9	7.2	3.7	2.6	.8	13.6	3.7	.6	6.8	9.7	1.8	1.3	3.9	3.5	7.7	6.4	1.0	2.6	2.8	5.3	4.5	8.1	4.9	1.6	8.7
10	.1	2.5	4.5	.8	9.[illegible]	8.2	1.6	4.3	13.8	2.5	2.3	3.6	1.7	2.9	5.1	.2	5.8	3.8	6.2	1.9	3.2	9.1	1.8	6.3
11	1.2	1.9	7.2	.8	5.4	8.9	1.4	.8	14.3	1.4	2.2	2.4	2.6	6.1	1.7	1.0	.1	4.7	6.0	4.0	3.1	11.8	1.4	3.8
12	2.1	5.1	6.9	1.8	2.0	6.5	1.1	2.6	6.0	.8	5.3	1.3	2.5	4.9	2.9	.9	2.1	6.7	4.7	7.0	6.2	10.4	5.5	1.9
13	4.1	3.9	6.7	1.7	.2	5.2	1.3	11.4	.6	3.9	4.1	1.2	.7	1.6	.4	2.0	4.1	6.4	3.6	7.8	7.0	4.1	9.3	.7
14	2.9	1.3	4.5	4.7	.2	3.0	1.2	11.0	1.5	3.8	.2	1.1	2.7	.5	4.3	2.9	3.0	7.2	.6	10.3	7.7	1.1	8.0	2.3
15	4.7	4.1	2.5	4.5	.8	2.0	.2	8.0	2.5	1.2	3.0	4.9	2.6	3.4	7.0	3.7	.1	6.9	.6	9.9	9.2	2.0	5.0	5.1
16	4.6	2.1	.5	4.3	1.7	2.8	.2	6.8	6.1	1.2	4.7	5.7	2.5	.5	5.0	.8	2.9	4.0	.6	6.1	8.9	1.0	2.0	5.0
17	2.6	1.6	4.0	4.2	1.7	2.7	.2	5.7	7.6	1.1	3.7	3.7	.6	1.4	2.1	1.9	5.4	2.0	1.3	3.3	7.8	3.6	4.6	.3
18	.8	4.1	4.7	.6	.7	2.6	.2	3.0	8.9	1.1	.1	1.0	.3	.5	2.0	3.6	5.2	.2	3.8	.5	2.4	5.2	7.8	3.2
19	.9	4.[illegible]	4.6	.3	.7	2.6	.2	1.2	7.9	1.1	1.6	.1	2.3	2.1	5.3	3.5	4.2	3.2	4.5	.5	2.4	2.5	6.8	2.3
20	.1	5.4	3.6	.5	.7	1.7	.2	3.0	4.5	1.8	4.0	.9	3.0	2.9	6.7	.9	5.7	3.1	4.4	2.8	1.5	1.6	4.2	.6
21	1.5	6.[illegible]	.4	2.1	.1	3.2	2.5	4.4	2.0	.6	2.3	.9	2.9	4.3	8.6	.7	7.7	3.8	3.5	4.3	3.8	.8	1.7	1.8
22	.7	3.6	2.7	4.5	.9	5.3	3.2	5.7	.3	3.6	1.5	.9	2.8	7.8	9.7	1.4	7.5	2.9	.5	1.8	4.4	2.3	.1	4.1
23	2.2	2.8	3.4	3.4	.1	5.1	3.1	6.3	6.8	7.0	2.2	.8	2.0	8.2	7.4	2.9	7.9	2.8	1.9	1.9	4.3	3.7	1.4	3.2
24	3.5	2.7	1.1	1.9	.6	5.0	5.8	4.7	8.5	8.7	2.8	.6	1.9	9.8	5.2	2.1	3.6	2.7	1.9	1.2	2.0	4.2	1.3	2.4
25	4.1	4.[illegible]	.4	2.5	.2	2.8	6.2	4.6	7.0	6.[illegible]	2.7	1.3	1.2	11.5	1.6	2.0	2.1	2.6	.4	1.8	2.6	3.4	.8	1.0
26	5.3	8.2	.4	2.5	.7	1.4	4.9	5.1	4.3	2.6	1.3	2.0	15.2	11.2	2.3	.7	2.1	2.6	1.3	1.2	1.4	.8	2.2	1.3
27	4.0	9.[illegible]	1.1	6.7	2.6	1.4	3.4	3.[illegible]	1.7	2.6	1.1	3.3	1.2	12.9	3.6	4.0	3.6	4.6	6.4	6.4	1.7	.9	.9	1.3

Table 6-3: Gore Centerline Error Angles, Circumferential Components

LEFT INTENTIONALLY BLANK

BEAN MAP OF TARGET AREA -UNITS ARE NO. OF BEANS

0	0	0	0	0	0	0	0	0	0
0	0	0	0	1	0	0	0	0	0
0	0	0	5	2	2	0	0	0	0
0	1	1	5	5	2	0	0	0	0
0	0	3	6	12	3	2	2	0	0
0	2	2	15	9	5	6	5	2	0
0	3	5	15	2	8	1	2	0	0
0	1	9	12	22	17	6	6	1	0
0	3	8	10	8	7	7	1	0	0
0	3	13	21	17	12	5	5	0	0
0	5	6	15	14	12	8	7	0	0
0	4	2[illegible]	10	7	1	7	3	2	0
0	2	2	4	[illegible]	1	[illegible]	1	0	0
0	0	0	4	1	4	5	1	0	0
0	0	0	0	4	4	[illegible]	0	0	0
0	0	0	0	0	0	0	0	0	0
0	0	0	0	0	0	[illegible]	0	0	0
0	0	0	[illegible]	[illegible]	[illegible]	[illegible]	[illegible]	0	0
0	0	0	0	[illegible]	0	0	0	0	0
0	0	0	0	0	0	0	0	0	0

TOTAL= 483.

Upper and lower receiver boundries

Circumferential spill-over

Table 6-4: "Bean Count" Map of Target Area

FLUX MAP OF TARGET AREA -UNITS ARE SQ. METER

0.000	0.000	0.000	0.000	0.000	0.000	0.000	0.000	0.000	0.000
0.000	0.000	0.000	0.000	.010	0.000	0.000	0.000	0.000	0.000
0.000	0.000	0.000	.057	.021	0.000	0.000	0.000	0.000	0.000
0.000	.000	.010	.050	.056	.024	0.000	0.000	0.000	0.000
0.000	0.000	.033	.073	.141	.040	.028	.021	0.000	0.000
0.000	.025	.019	.179	.101	.058	.069	.052	.025	0.000
0.000	.022	.050	.136	.023	.085	.012	.017	0.000	0.000
0.000	.005	.074	.123	.233	.170	.063	.066	.012	0.000
0.000	.021	.079	.116	.073	.071	.050	.009	0.000	0.000
0.000	.021	.099	.163	.116	.099	.039	.038	0.000	0.000
0.000	.039	.033	.099	.082	.069	.054	.044	0.000	0.000
0.000	.019	.104	.057	.049	.007	.038	.013	.011	0.000
0.000	.010	.009	.021	0.000	.006	0.000	.003	0.000	0.000
0.000	0.000	0.000	.017	.003	.015	.019	.004	0.000	0.000
0.000	0.000	0.000	0.000	.016	.016	0.000	0.000	0.000	0.000
0.000	0.000	0.000	0.000	0.000	0.000	0.000	0.000	0.000	0.000
0.000	0.000	0.000	0.000	0.000	0.000	0.000	0.000	0.000	0.000
0.000	0.000	0.000	0.000	0.000	0.000	0.000	0.000	0.000	0.000
0.000	0.000	0.000	0.000	0.000	0.000	0.000	0.000	0.000	0.000
0.000	0.000	0.000	0.000	0.000	0.000	0.000	0.000	0.000	0.000

Table 6-5: Flux Map of Target Area

The flux map is further illustrated by the three dimensional plot in Figure 6-4. The data of Table 6-5 were used. Spill-over in the circumferential direction outside of the 5 column area encompassing the aim points was added in on the opposite side, assuming three identical cycles of this flux map around the receiver. This plot reveals the nonuniform nature of the flux distribution within the receiver area.

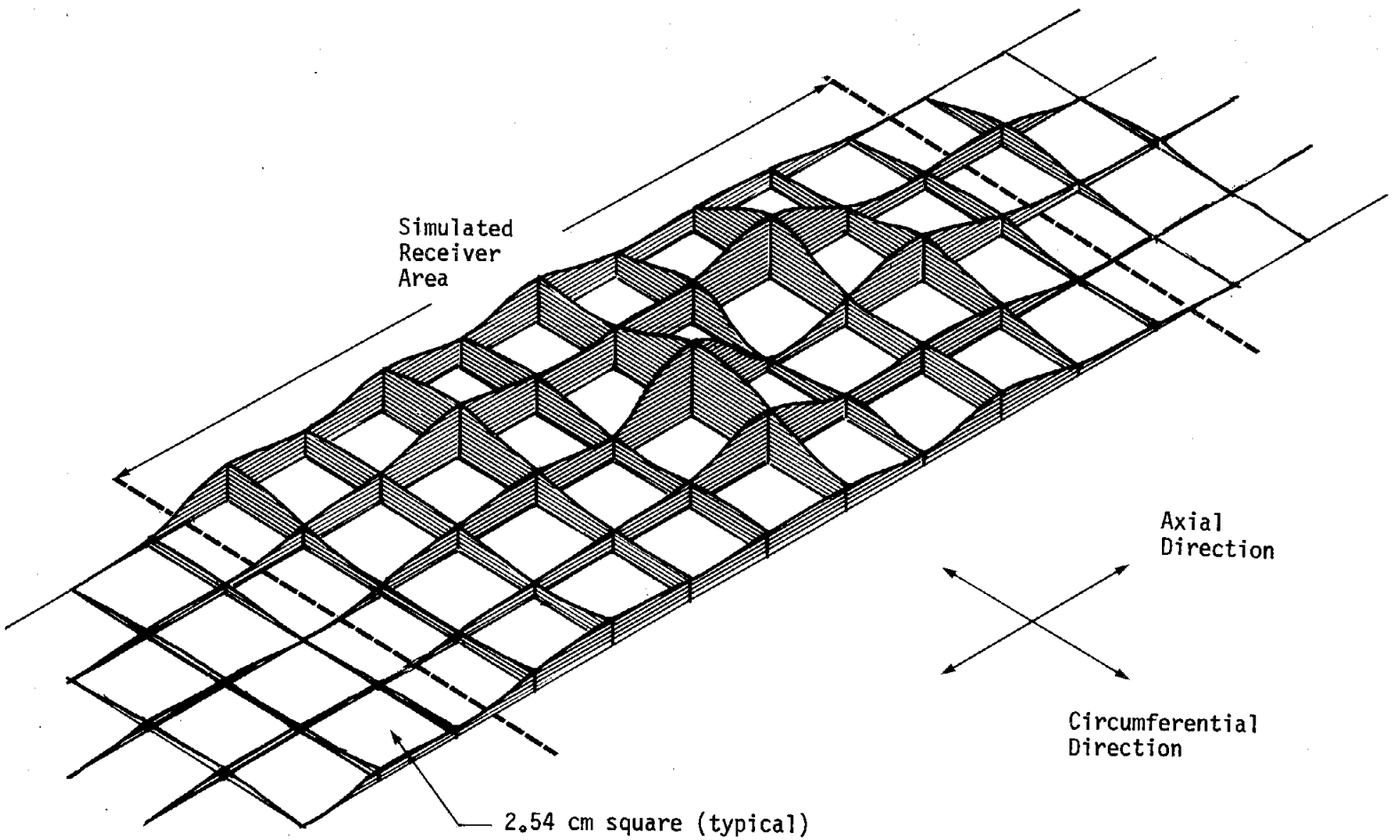

Figure 6-4: Plot of Flux Map Data

7.0 CONCLUSIONS

The objective of the program was to design and evaluate a photovoltaic concentrator using a plastic film reflector. A prototype concentrator was built incorporating the key design features. The deep dish configuration with a cylindrical photovoltaic cell receiver was selected as the concentrator configuration because it was predicted to have a high energy intercept factor, good solar cell module configuration and a large active reflective area.

Three 4 m diameter reflectors were fabricated to enable experimental determination of the illumination flux on the receiver by use of a laser ray trace. Fabrication of more than one reflector was necessary because results were not satisfactory, and corrections in deficient areas were attempted.

Efforts to improve performance of the reflector by changing the gore segment width, fabrication techniques, and assembly procedures provided improvements to specific problem areas. However, these efforts were largely unsuccessful in fulfilling the most important objective, optical performance needed for efficient receiver operation. All of the reflectors exhibited optical performance inadequate for efficient operation where both a high intercept factor and uniform energy distribution is required.

The disappointing results can be attributed to several factors. Plastic film reflectors with a short focal length, deep-dish configuration proved to be much more difficult to assemble than the previously fabricated parabolas with a f/D = .5. The difficulties are due to reduced accessibility to the work, more curvature in the radial direction, and increased angular change across seam locations of the lay up tool. The fabrication and assembly techniques were based on those successfully used to build a reflector of comparable size but with f/D = .5. This approach relies on accurate cutting and joining of the gore segments to obtain the desired concentrator shape, instead of using an accurately made lay-up tool to define the shape. The required accuracies could not be obtained with the increased assembly difficulties noted above.

Major expansion of the effort would be needed to overcome the difficulties encountered. In particular, high accuracy lay-up tooling would be necessary, and the tool would probably have to include vacuum hold-down over

the entire gore surface, built in gore edge trimming, and equipment for automatically aligning and applying the seam tape under uniform tension. A detailed process development program would be required to assure accurate and structurally adequate joints.

8.0 REFERENCES

1. Plastic Parabolic Concentrator Feasibility Study, Sandia Report No. Sand 79-7004, prepared by Boeing Engineering and Construction, January 1979, Sandia Contract No. 05-4467.

2. D. K. Zimmerman, "Evaluation of a Plastic Parabolic Concentrator for Terrestial Photovoltaic Application", 13th IEEE Photovoltaics Specialists Conference, June 1978.

3. Solar Central Receiver Prototype Heliostat, Volume I, Final Report, Sandia Report No. SAN-1604-1, prepared by Boeing Engineering and Construction June, 1978, DOE Contract No. EG-77-C-03-1604.

4. Low Cost Point Focus Solar Concentrator, Phase 1, Final Report, prepared by Boeing Engineeirng and Construction, March 1979, JPL Contract No. 955209.

5. Plastic Film Performance Improvement for Heliostats, Final Report, prepared by Boeing Engineering and Construction, July 1980, Sandia Contract No. 83-0035D.

DISTRIBUTION LIST:

Acurex Corporation (3)
Attn: George Sutton
Bob Spencer
John Kull
485 Clyde Avenue
Mountain View, CA 94042

Aerospace Corporation
Attn: Ed Simburger
2350 El Segundo Blvd.
El Segundo, CA 90266

Alliance Tool Corp.
Fresnel Optics Division
Attn: Helmut Walter
1300 Mt. Read Blvd.
Rochester, NY 14606

Applied Solar Energy Corp. (3)
Attn: Steve Olah
Frank Ho
Ken Ling
15251 E. Don Julian Road
City of Industry, CA 91746

ARCO Power Systems
Attn: Floyd Blake
Suite 307
7061 S. University Blvd.
Littleton, CO 80122

Arizona State University (2)
Attn: Charles Backus
Robert Sanderson
College of Engineering
Tempe, AZ 85281

Ray Bahm & Associates
Attn: Ray Bahm
2513 Kimberly Court NW
Albuquerque, NM 87130

Battelle
Attn: Don Carmichael
505 King Avenue
Columbus, OH 43201

The BDM Corporation (3)
Attn: Tim Lambarski
Wayne Kauffman
Bill Schwinkendorf
1801 Randolph Road SE
Albuquerque, NM 87111

Boeing Engineering & Const. Co. (10)
Attn: Roger Gillette
P. O. Box 3707
Seattle, WA 98124

Burns & Roe, Inc. (2)
Attn: G. A. Fontana
800 Kinderkamack Road
Oradell, NJ 07649

Chevron Research (2)
Attn: John Cape
R. Creek
576 Standard Avenue
Richmond, CA 94802

Cyro Industries
697 Route 46
Clifton, NJ 07015

U. S. Dept. of Energy (2)
ALO
Attn: James Morley
Ethan Walker
P. O. Box 5400
Albuquerque, NM 87115

U. S. Dept. of Energy (8)
Div. of PV Energy Technologies
Attn: R. Annan
M. B. Prince
L. Herwig (5)
A. Scolaro
1000 Independence Ave. SW
Washington, DC 20585

U. S. Dept. of Energy
Attn: John Hanson
Nuclear & Geosciences Div.
P. O. Box 5400
Albuquerque, NM 87115

E-Systems (2)
Attn: Mark O'Neill
A. J. McDanal
P. O. Box 226118
Dallas, TX 75266

General Electric Co.
Attn: Ron Hodge
P. O. Box 527
King of Prussia, PA 19406

International Rectifier
Attn: Harold Weinstein
235 Kansas Street
El Segundo, CA 91214

Intersol Power Corporation
Attn: John Sanders
7400 W. Radcliff Avenue
Littleton, CO 80123

Jet Propulsion Lab (3)
Attn: K. Shimada
R. Ferber
Solar Data Center
4800 Oak Grove Drive
Pasadena, CA 91109

Martin Marietta (4)
Attn: S. Broadbent
R. Hein
D. Hughes
J. Baumann
P. O. Box 179
Denver, CO 80201

Microwave Associates
Attn: Jonathon Chapple-Sokol
South Avenue MS-116
Burlington, MA 01803

McGraw Hill
607 Boylston St.
Boston, MA 02116

3M
Attn: Sanford Cobb
Industrial Optics
235 2D15
3M Center
St. Paul, MN 55144

Motorola
Attn: Keith Kingston
GED
8201 E. McDowell
Scottsdale, AZ 85252

NASA, HQ
Attn: John Loria
Code RET-1
Washington, DC 20546

New Shelter Home Magazine
9317 Shoshone
Albuquerque, NM 87111

Oak Ridge National Lab
Attn: Steve Kaplan
P. O. Box X
Oak Ridge, TN 37830

Oklahoma University
571 South University Blvd.
Norman, OK

Photowatt (2)
Attn: William Taylor
Mike Keeling
2414 W. 14th Street
Tempe, AZ 85281

Power Hybrids
Attn: Jeff Meyer
1742 Crenshaw Blvd.
Torrance, CA 90501

PRC
Attn: E. Stirewalt
5201 Leesburg Pike
Suite 400
Falls Church, VA 22070

Purdue University (2)
Attn: Richard Schwartz
Mark Lundstrom
Electrical Engineering Dept.
West Lafayette, IN 47907

Quantum Specialties
Attn: James E. Molle
163 Verde Circle
Rohnert Park, CA 94928

Research Triangle Institute
Attn: Mayrant Simons
Box 12194
Research Triangle Park, NC 27709

SERI (3)
Attn: Gene Blakeslee
Lee Cole
John Benner
1617 Cole Blvd.
Golden, CO 80401

SERI, Library (2)
1536 Cole Blvd., Bldg. #4
Golden, CO 80401

Southern Cal Edison
Attn: Spencer Carlisle
2244 Walnut Grove Ave.
Rosemead, CA 91770

Spectrolab
Attn: Brian Elm
12500 Gladstone Avenue
Sylmar, CA 91342

Spire (3)
Attn: S. Tobin
M. Nowlan
R. Little
Patriots Park
Bedford, MA 01730

Star Light Energy
Attn: J. Furber
1717 18th Street NW
Washington, DC 20009

Strategies Unlimited
201 San Antonio Circle
Suite 205
Mountain View, CA 94040

Solar Works
Attn: Paul Wilkins
Route 2, Box 274
Santa Fe, NM 87501

Thermo Electron
Attn: Ron Scharlack
45 First Avenue
Waltham, MA 02154

UNM/NMERI
Attn: G. Leigh
Campus Box 25
Albuquerque, NM 87131

Varian & Associates (2)
Attn: Peter Borden
N. Kaminar
611 Hansen Way K-219
Palo Alto, CA 94303

University of Wisconsin
Attn: Prof. J. D. Wiley
Dept. of Electrical Engineering
Madison, WI 53706

Wright Patterson AFB
Attn: Jack Geis
AFWAL/POOC
Wright Patterson AFB, OH

Wyle Labs (2)
Attn: Dave Christenson
George Meares
7800 Governors Drive West
Huntsville, AL 35807

1133 R. Chaffin
1133 J. Wiczer
1811 R. Assink
1822 J. Sweet
Attn: M. Moss
R. Pettit
1823 M. Chamberlain
1845 R. Eagan
2142 B. Rose
2146 M. Garner
2146 B. Hanson
2146 B. Nasby
2146 J. Rodriguez
2146 H. Weaver
9700 E. Beckner
9720 D. Schueler
9721 J. Banas
9721 H. Gerwin
9723 E. Burgess
9724 E. Boes
9724 D. Arvizu
9724 L. Beavis
9724 C. Chiang
9724 M. Edenburn
9724 D. King
9724 A. Maish
9724 M. Rios
9724 C. Stillwell
3141 L. J. Erickson (5)
3151 W. L. Garner (3)
3154-3 C. H. Dalin (25)
For DOE/TIC (Unlimited Release)
8214 M. A. Pound